Biochemistry and Biophysics Reports 39 (2024) 101745

Contents lists available at ScienceDirect

Biochemistry and Biophysics Reports

journal homepage: www.elsevier.com/locate/bbrep

Development of an ancestral DC and TLR4-inducing multi-epitope peptide vaccine against the spike protein of SARS-CoV and SARS-CoV-2 using the advanced immunoinformatics approaches

Cena Aram [a], Parsa Alijanizadeh [b,c], Kiarash Saleki [b,c,*], Leila Karami [a,**]

[a] Department of Cell & Molecular Biology, Faculty of Biological Sciences, Kharazmi University, Tehran, Iran
[b] Student Research Committee, Babol University of Medical Sciences, Babol, Iran
[c] USERN Office, Babol University of Medical Sciences, Babol, Iran

ARTICLE INFO

Keywords:
Immunoinformatics
Multi-epitope
SARS-CoV
Reverse vaccinology
SARS-CoV-2
Computational immunology

ABSTRACT

The oldest human coronavirus that started pandemics is severe acute respiratory syndrome virus (SARS-CoV). While SARS-CoV was eradicated, its new version, SARS-CoV2, caused the global pandemic of COVID-19. Evidence highlights the harmful events orchestrated by these viruses are mediated by Spike (S)P protein. Experimental epitopes of the S protein which were overlapping and ancestral between SARS-CoV and SARS-CoV-2 were obtained from the immune epitopes database (IEDB). The epitopes were then assembled in combination with a 50 S ribosomal protein L7/L12 adjuvant, a *Mycobacterium tuberculosis*-derived element and mediator of dendritic cells (DCs) and toll-like receptor 4 (TLR4). The immunogenic sequence was modeled by the GalaxyWeb server. After the improvement and validation of the protein structure, the physico-chemical properties and immune simulation were performed. To investigate the interaction with TLR3/4, Molecular Dynamics Simulation (MDS) was used. By merging the 17 B- and T-lymphocyte (HTL/CTL) epitopes, the vaccine sequence was created. Also, the Ramachandran plot presented that most of the residues were located in the most favorable and allowed areas. Moreover, SnapGene was successful in cloning the DNA sequence linked to our vaccine in the intended plasmid. A sequence was inserted between the *Xho*I and *Sac*I position of the pET-28a (+) vector, and simulating the agarose gel revealed the existence of the inserted gene in the cloned plasmid with SARS vaccine (SARSV) construct, which has a 6565 bp in length overall. In terms of cytokines/IgG response, immunological simulation revealed a strong immune response. The stabilized vaccine showed strong interactions with TLR3/4, according to Molecular Dynamics Simulation (MDS) analysis. The present ancestral vaccine targets common sequences which seem to be valuable targets even for the new variant SARS-CoV-2.

1. Introduction

The coronavirus causing severe acute respiratory syndrome (SARS-CoV) initially appeared in 2003 [1]. World Health Organization (WHO) estimates that approximately 8000 people were infected and about 700 were killed during the first Coronavirus pandemic in 2002–2003 [2]. SARS-CoV has 79 % genomic overlap with SARS-CoV-2 [3]. Oftentimes, SARS-CoV presents in its severe form and other symptoms such as, muscle pain, headache, fever, mainly cough, dyspnea, and pneumonia are similar to SARS-CoV-2 [4]. Alternatively, SARS-CoV-2, whose dissemination killed more than 14.9 million people worldwide [5] as a result of many pandemics, launched a tragedy in 2019 in Wuhan, China. More recently, the subvariant of the omicron virus emerged [6]. Coronaviruses (CoVs) can infect humans as well as wild animals [7]. Positive-sense, single-stranded RNA virus referred to SARS-CoV-2 penetrates respiratory system cells by employing mechanisms similar to those in SARS-CoV [8,9], SARS-CoV is a human CoV meaning it can affect humans. Human CoVs also include HCoV-229 E, HCoV-NL63, HCoV-OC43, HCoV-HKU1, MERS-CoV, and SARS-CoV-2 [10]. The SARS-CoV genome is approximately 30 Kb in size and comprises 14 possible open reading frames (ORFs). SARS-CoVs are + ssRNA viruses, and the virion is made up of a nucleocapsid (N) core that is surrounded by three structural proteins: the spike (S), membrane (M), and envelope (E) protein [11] which are widespread throughout all genera, including

* Corresponding author. Babol University of Medical Sciences, Babol, Iran.
** Corresponding author.
E-mail addresses: k.saleki@mubabol.ac.ir, kiarash_saleki@icloud.com (K. Saleki), l_karami@khu.ac.ir (L. Karami).

https://doi.org/10.1016/j.bbrep.2024.101745
Received 12 March 2024; Received in revised form 26 April 2024; Accepted 29 May 2024

SARS-CoV-2 and MERS-CoV. The most important and well-known component of CoVs for focusing any therapy that plays a key part in infection and cellular immune feedback is the S protein [12]. S protein is able to bind cellular receptors [13]. S1 and S2 make up the structure of the S protein. Angiotensin-converting enzyme 2 (ACE2) receptor attachment is enhanced through S1 [14] and S2 contains fusion peptides [15]. The S protein is crucial for the activation of T-cell responses and neutralizing antibodies [14] that detected the significance of the S protein. However, the S protein in SARS-CoV-2 has a somewhat variable sequence which makes different pandemics and variants of concern such as Alpha, Beta, Gamma, Delta, and especially Omicron that spike aimed at viruses to avoid the immunological mechanisms [16]. Various suitable immunotherapies have been engineered through different technologies, like mRNA vaccine (Pfizer-BioNTech and Moderna) [17,18], Adenovirus vector vaccine (Oxford-AsteraZeneca, Sputnik V, and Janssen (Johnson & Johnson)) [19], inactivated virus vaccine (Sinopharm and Covaxin) [20,21], subunit vaccine (Novavax) [22], and other vaccines. Most platforms of vaccine candidates in clinical trials are concentrated on CoV S protein [23]. We investigated the S protein in this study. In the previous studies, immunoinformatics methods were used to target the viral antigens, predict epitopes and assess their suitability as vaccine components [24]. By predicting the prospective candidate peptides in conjunction with adjuvants to augment the immune feedback against any viruses, the bioinformatics technique can speed up the vaccine development phases. An effective multi-epitope vaccine against other CoVs (MERS-CoV), Ebola virus, Zika virus, and emergence Monkeypox virus has been the subject of earlier investigations employing immunoinformatics [25–28]. We investigated SARS-CoV using a new approach that takes into account the significance of vaccines for future variants of human CoVs. This work aimed to create an ancestral SARS multi-epitope vaccine for SARS-CoV and SARS-CoV-2 based on the immunoinformatics and structural bioinformatic tools utilizing the experimental MHC I/II, and B-cell epitopes of the S antigen in SARS-CoV/SARS-CoV2 viruses.

2. Materials and methods

2.1. Acquisition and assessment of epitopes

SARS-CoV experimental epitope sequence was acquired from IEDB (https://www.iedb.org/) (ID:10002316). IEDB was used to obtain 486 epitope sequences, including 34 MHC I, 40 MHC class II, and 412 B-lymphocyte epitopes. In general, our workflow to engineer a chimeric immunogenic protein for SARS-CoV and SARS-CoV-2 (SARS-vaccine) is demonstrated in Fig. 1.

2.2. Forecasting of antigenicity, allergenicity, toxicity, and water-soluble analysis

Antigenic potential of epitopes was first investigated by VaxiJen v2.0 tool [29] with the model set to virus module. We tested if the collected epitopes could be allergenic by AllerTop v.2.0 [30]. Only the epitopes identified as non-allergen are chosen for the following study. The ToxinPred tool [31] was employed to evaluate the toxic epitopes, Using the default settings. In addition, Virulentpred [32] (SVM based with default parameters) that can aid to find out the novel target for designing the protective multi-epitope vaccine and then evaluated the rest of the antigenic and non-toxic/allergen epitopes. The subsequent assessment was limited to the epitopes classified as virulent. Non-soluble epitopes were filtered using the innovagen website's proteomics-tools (http://www.innovagen.com/proteomics-tools).

2.3. Conservancy, non-homology, SARS-CoV-2 similarity, and physicochemical features

Using the IEDB Conservancy Tool and a 100 percent identity setting, a selection of epitope sequences was matched to the source protein sequences. A computational score for conserved epitopes evaluated within SARS-CoV spike protein through IEDB and Analysis Resource epitope conservancy tool (http://tools.iedb.org/conservancy/). SARS-CoVs protein sequences (Uniprot Reference Sequence: P59594) were obtained in FASTA format from the Uniprot Reference Sequence Database

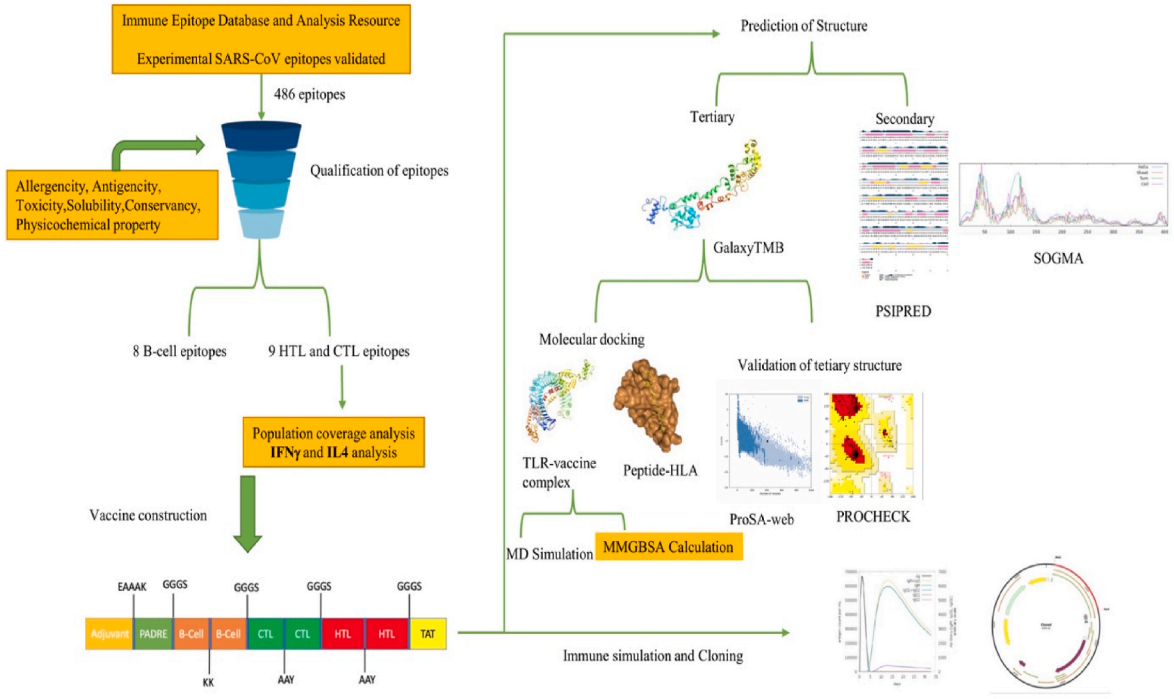

Fig. 1. The strategy of designing multi-epitope vaccine for SARS-CoV and SARS-CoV-2.

Table 1
SARS-CoV-2 homology, immunological and physico-chemical properties of experimental evaluated epitopes in SARS-CoV. ([1] MHC I,[2] MHC II, * B-cell, AT: Antigenicity, T/A: Toxicity/Antigenicity, NTA: Non-Toxin/Allergen, MW: Molecular Weight, AI: Aliphatic Index, II: Instability Index).

Epitope Id	Conserved Epitope	Position	SARS-CoV-2 Homology	AT	IL4 Inducer	T/A	Solubility	Virulence	MW	AI	Half-Life	II
7382	CYGVSATKL[1]	366-374 (RBD)	yes	1.3964	–	NTA	Soluble	1.053	941.11	86.67	1.2	−9.98
30,098	KCYGVSATKL[1]	365-374 (RBD)	yes	1.2559	+	NTA	Soluble	1.068	1069.28	78	1.3	−7.98
46,680	NYNYKYRYLR[1]	435-444 (RBD)	yes	0.9134	+	NTA	Soluble	1.0606	1452.64	39	1.4	3.81
59,162	SLIDLQELGKYEQYIKW[1]	1178-1194 (S2)	yes	1.3608	+	NTA	Soluble	1.0602	2126.44	114.71	1.9	32.39
187,223	HNYKYRYL[1]	436-443 (RBD)	yes	0.7747	+	NTA	Soluble	1.0606	1156.31	48.75	3.5	7.79
Epitope Id	**Epitope**	**Position**	**SARS-CoV-2 Homology**	**AT**	**IFNγ**	**T/A**	**Solubility**	**Virulence**	**MW**	**AI**	**Half-Life**	**II**
21,552	GNYNYKYRYLRHGK[2]	434-448 (RBD)	yes	1.105	+	NTA	Soluble	1.0606	1945.21	52	30	−5.18
30,098	KCYGVSATKL[2]	365-374 (RBD)	yes	0.799	–	NTA	Soluble	1.068	1069.28	78	1.3	−7.98
100,481	RPFERDISNVPFS[2]	449-451 (RBD)	yes	0.56	+	NTA	Soluble	1.0525	1563.73	52.31	1	68.49
46,680	NYNYKYRYLR[2]	435-444 (RBD)	no	0.635	+	NTA	Soluble	1.0606	1452.64	39	1.4	3.81
Epitope Id	**Epitope**	**Position**	**SARS-CoV-2 Homology**	**AT**		**T/A**	Soluble	**Virulence**	**MW**	**AI**	**Half-Life**	**II**
1410725	ALVNSQCDLTGR*	10-21 (S1)	yes	1.30		NTA	Soluble	1113	1276.43	97.5	4.4	27.91
1438973	GDCLGGISARDL*	811-822 (S2)	yes	1.19		NTA	Soluble	1.0681	1176.31	105.83	30	28.43
1440344	GGISARDLICAQ*	815-826 (S2)	yes	1.70		NTA	Soluble	1.0622	1203.38	114.17	30	12.38
1469577	LLTIHRGDPMPN*	240-251 (S1)	yes	0.99		NTA	Soluble	1.0636	1363.6	97.5	5.5	42.71
1474380	LVNSQCDLTGRT*	11-22 (S1)	yes	1.24		NTA	Soluble	1.0526	1306.46	89.17	5.5	27.91
1503320	SETKCTLKSLSV*	292-303 (S1)	yes	1.06		NTA	Soluble	1.0602	1295.51	8917	1.9	45.31
1534769	YGDCLGGISARD*	810-821 (S2)	yes	1.14		NTA	Soluble	1.0733	1226.33	73.33	2.8	21.35
7868	DDSEPVLKGVKLHYT*	1241-1255 (S2)	yes	1.18		NTA	Soluble	1.0122	1700.91	90.67	1.1	65.43

(https://www.uniprot.org/) that certain about conservancy. Selected epitopes were aligned to Homo sapiens (taxid:9606) in BLASTp [33] in order to detect the non-homology between the human proteins and epitopes to avoid autoimmune and omit epitopes that has similarities with the human proteins. Accordingly, epitopes aligned to SARS-CoV-2 (taxid:2697049) to make a vaccine is effective in two spices and characterized the ancestral epitopes among SARS-CoV/SARS-CoV-2. The Expasy ProtParam tool (https://web.expasy.org/protparam/) was used to assess physico-chemical characterization of the submitted epitopes, in addition to their stability and molecular weight.

2.4. Conserved position of spike protein in different variant of SARS-CoV-2 and SARS-CoV

Initially, we gathered 18 distinct SARS-CoV-2 and SARS-CoV protein sequences from the NCBI virus database, which is scheduled for publication in 2023. Several SARS-CoV-2 variants, include Alpha, Beta, Delta, Omicron, and sub-lineages of Omicron that extracted that referred in supplementary data. The variants of SARS-CoV-2/SARS-CoV are provided in Table S1, and we used MEGA11 [34] to multiple align the sequences with the MUSCLE algorithm in order to analyze and show a phylogenetic tree.

2.5. Prediction of IL4 and IFNγ in MHC I/II epitopes

For the purpose of anticipate the IL4 inducer in the MHC I epitope, the chosen epitopes were examined by IL4Pred (http://crdd.osdd.net/raghava/il4pred/). IFNepitope server (http://crdd.osdd.net/raghava/ifnepitope/) was used to forecast the IFN-triggering epitopes. In order to forecast the possible of the peptide to induce IFN-γ and IL4, the online web servers IFNepitope and IL4Pred use a variety of algorithms, including motif-based search, machine learning, and hybrid approaches.

2.6. Building a multi-epitope peptide SARS chimera

For creating the effective SARSV vaccine (SARS vaccine) construct, the final subunit vaccine model was created via merging chosen epitopes by different linkers and adjuvants. To increase immunogenicity, a substantial immunostimulatory adjuvant was applied to the multi-epitope [35]. This work demonstrated that dendritic cells (DCs) triggered by *Mycobacterium tuberculosis* Rv0652 may significantly polarize CD4+/CD8+ T-lymphocytes to release IFN-gamma as well as trigger T-lymphocytes-regulated cell killing in reply to the induction of naive T-lymphocytes [36]. Initially, a rigid linker named the EAAAK linker was utilized to connect the adjuvant to the vaccine sequence N-ending. To further boost vaccine immunogenicity, the pan-HLA DR binding epitopes (PADRE epitope 13aa) sequence was added after this linker [37]. Linkers are necessary for separating functional domains, establishing extended conformation, and folding proteins, all of which lead to become steady protein structure [38]. In mammalian cells, AAY (Ala-Ala-Tyr) linkers are the site of proteasome cleavage. The AAY linkers assist in the formation of epitopes in a natural form and prevent the formation of junctional epitopes, which enhanced their presentation [39,40]. In addition to providing efficient separation of functional domains, EAAAK linkers also contribute to flexibility, folding activities, and the separation of functional domains in epitopes [41]. It is common to include Gly and Ser in the linker sequence of GGGS proteins in order to provide additional flexibility to that region. As a result of the Gly

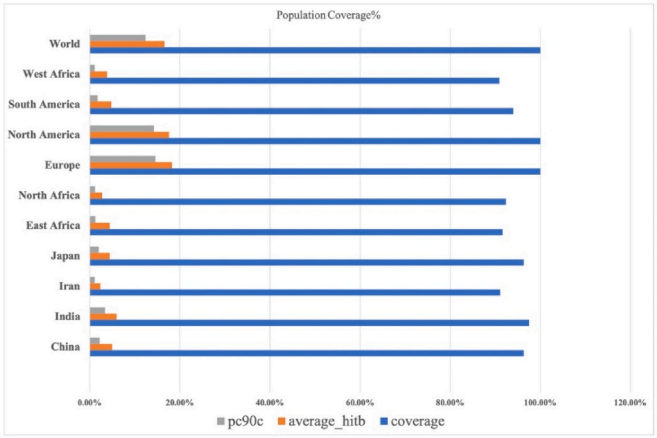

Fig. 2. Analysis of vaccine population coverage. Population coverage of different country: China 96.29 %, East Africa 91.61 %, Europe: 100 %, India: 97.49 %, Iran: 91.12 %, Japan: 96.33 %, North Africa: 92.37 %, South America: 94.01 %, West Africa 90.87 %.

Table 2
The selected epitope coverage in the world.

Class I Epitope	Coverage
KCYGVSATKL	63.32 %
CYGVSATKL	48.75 %
NYNYKYRYLR	24.08 %
SLIDLQELGKYEQYIKW	60.68 %
HNYKYRYL	73.35 %
Class II Epitope	**Coverage**
GNYNYKYRYLRHGKL	100 %
KCYGVSATKL	100 %
RPFERDISNVPFS	100 %
NYNYKYRYLR	100 %
Epitope set	**100 %**

residue in particular, the linker region will remain flexible and not fold into a secondary structure that is difficult to access [42]. B-cell epitopes were also bound using KK linkers. Cathepsin B, one of the key proteases for antigen processing in the context of MHC-II antigen presentation, is the KK linker of the lysosomal protease target sequence [43,44]. The CTL or major histocompatibility complex I (MHC-I) epitopes were connected through the AAY linker, followed by the Helper T cell (HTL) epitopes by AAY connectors. The B-lymphocyte epitopes were coupled using KK connector. The GGGS linker split the epitope class [37]. The vaccine's C-terminal was finally modified with TAT (11 aa), the intended construct's sequence for greater cell penetration [45].

2.7. Proteosome cleavage

T-cell epitopes and the C-terminus of MHC I/II peptide ligands are produced by the proteasome complex, which is primarily in charge of the proteolytic degradation of cytosolic proteins. Proteasomal cleavage site prediction is therefore important for predicting T-cell epitopes. The PCPS [46], a popular tool for predicting proteasomal cleavage sites (http://imed.med.ucm.es/Tools/pcps/), was used in this investigation. To predict the number of cleavage sites per residue and the peptides containing cleavage sites at C-teminus, we employed the Immunoproteasome model.

2.8. Coverage assessment in human population

Using IEDB server (http://tools.iedb.org/population/), we assessed the coverage of selected epitopes in selected HLA classes within the target population and calculated IC_{50} thresholds for the selected epitope based on the IEDB's SMM algorithm (http://tools.immuneepitope.org/mhci/) and we use the class I and II combine calculation option. The reference alleles that selected are HLA-A*01:01, HLA-A*23:01, HLA-A*24:02, HLA-A*26:01, HLA-A*29:02, HLA-A*30:02, HLA-A*03:01, HLA-A*30:01, HLA-A*11:01, HLA-A*31:01, HLA-A*33:01, HLA-A*01:03, HLA-A*01:06, HLA-A*01:09, HLA-A*01:23, HLA-A*02:01, HLA-A*02:02, HLA-A*02:03, HLA-A*02:04, HLA-A*02:05, HLA-DMA*01:01, HLA-DMA*01:02, HLA-DMA*01:03, HLA-DMA*01:04, HLA-DMB*01:01, HLA-DMB*01:02, HLA-DMB*01:03, HLA-DMB*01:04, HLA-DPA1*01:03, HLA-DPA1*01:04, HLA-DPA1*01:05, HLA-DPA1*01:07. The MHCcluster 2.0 server (http://www.cbs.dtu.dk/services/MHCcluster/) was used in this work to construct phylogenetic tree-based visualizations and heat maps of the functional cluster between the MHC variations using the default features [47]. An HLA corresponding module was used to apply the NetMHCpan-2.8 technique for MHC-I cluster evaluation, whereas HLA-DR representatives allele modules were chosen for MHC-II cluster evaluation.

2.9. Assessment of antigenicity, allergenicity, toxicity, solubility, and physico-chemical of multi-epitope vaccines

The section evaluated the toxicity and allergenicity by using the ToxinPred and AllerTop web servers after initially predicting the antigenicity with VaxiJen. The Protein-Sol method was utilized to estimate the vaccine construct's solubility [48] and SOLpro [49] web servers were used. There were SOLpro [39] web servers in use. The solubility of protein data from the E. coli expression system were predicted by the Protein-Sol service. The solubility of a protein sequence is forecasted by SOLpro using an SVM-based method. The Expasy ProtParam program (https://web.expasy.org/protparam/) was operated to estimate a number of physicochemical properties, including molecular weight, the Grand Average of Hydropathicity (GRAVY), theoretical isoelectric point (pI), instability index, aliphatic index, and half-life.

2.10. Anticipating of secondary structure and SARSV protein disorder areas

SOPMA (https://npsa-prabi.ibcp.fr/cgi-bin/npsa automat. pl?page = /NPSA/npsa sopma. html) and PSIPRED (http://bioinf.cs.ucl.ac.uk/psipred/) web servers were employed to estimate the secondary construct of multi-epitope immunogen as a means to a ratio of Helix, sheet, Turn, and Coil. Predicting the non-structured/disorder sections, mRNA expression, nucleic acid, stability, along with folding of the produced protein, which may be altered by low complexity of the sequence and areas with considerable flexibility called disorder areas, is a critical experiment in immunoinformatic and vaccine evolution. To forecast the disorder locations, DisEMBL 1.5 (http://dis.embl.de/) and DISOPRED3 (http://bioinf.cs.ucl.ac.uk/psipred/) were used.

2.11. 3D modeling, refinement, and quality confirmation of the tertiary construct

GalaxyTMB server (https://galaxy.seoklab.org/cgi-bin/submit.cgi?type=TBM) was utilized to estimate the tertiary structures of multi-epitopes and construct 3D models. This service uses *ab initio* modeling to enhance the loop or terminal areas in the primary 3D model used by GalaxyRefine (https://galaxy.seoklab.org/cgi-bin/submit.cgi?type=REFINE). Additionally, the ProSA-web (https://prosa.services.came.sbg.ac.at/prosa.php) and ERRAT (https://saves.mbi.ucla.edu/) were used to validate the projected tertiary structure. ProSA-Z-score web's measures the total and local model quality. The result of ERRAT and PROCHECK Ramachandran plots were displayed together to illustrate the favorable areas, extra authorized regions, and banned regions [50].

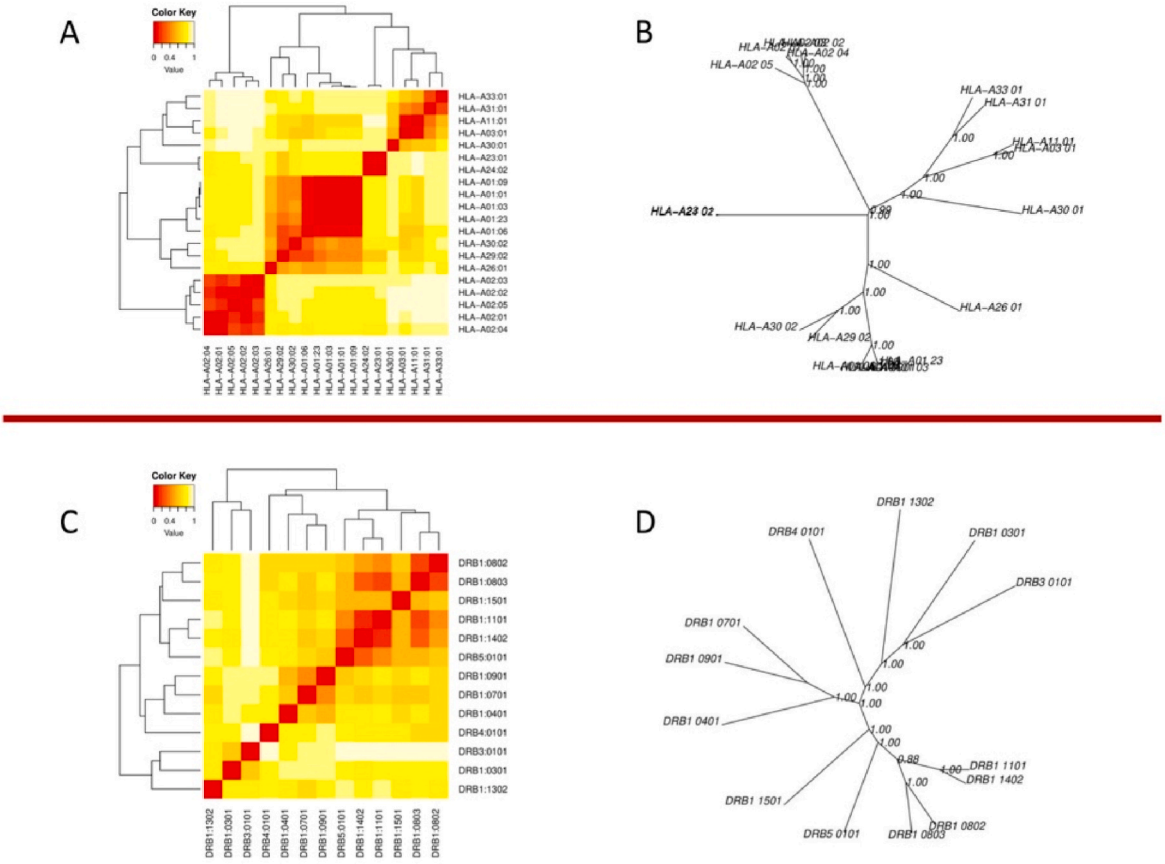

Fig. 3. MHC I and MHC II cluster analysis. **A**: MHC class I cluster analysis heatmap **B**: MHC I cluster analysis advanced tree map **C**: MHC class II cluster analysis heatmap **D**: MHC class II cluster analysis advanced tree map.

2.12. Prediction of conformational/linear B-lymphocyte epitopes

The B-cells lie at the center of immune response and interaction with the antigen and its participation is essential for the development of a robust immune response as well as a long-lasting memory. B-cell epitopes play a major role in the identification of antigens as well as interplay with antibodies. The discontinuous B-cell epitope contained in the vaccine design was predicted using the ElliPro web tool (http://tools.iedb.org/ellipro/), with default parameters (minimum 0.5, maximum 0.6) [51]. The Bcepred tool (https://webs.iiitd.edu.in/raghava/bcepred/bcepred) was utilized to predict continuous B-lymphocyte epitopes in antigenic sequences by physico-chemical properties. Prediction features analyzed comprised hydrophilicity, exposed surface, antigenic propensity, accessibility, flexibility, turns, and polarity. The default setting for Bcepred analyses was used.

2.13. Modeling of peptide and docking with MHC-I/II

PEP-FOLD 3.0 software chose the last 2 corresponding CTL and HTL epitopes as models [52]. The HDOCK server's protein-protein docking method was utilized to obtain suitable molecular docking between CTL/HTL epitopes and MHC I and II molecules (HLA-A*0201 (PDB:4U6X) and HLA-DRB1*0101 (PDB:2FSE)). After then, the PRODIGY was implemented to calculate the binding affinity [53].

2.14. Vaccine-TLR3/4 docking

The molecular docking method was utilized to evaluate the reaction of the vaccine and the Toll-Like Receptors [TLR3 (PDB:2A0Z), TLR4 (PDB:3FXI)]. We employed HDOCK, a hybrid template-reliant modeling and *ab initio* free approach for protein-protein docking [54]. Then PDBsum server [55] utilized for the vaccine-receptor contacts analysis, based on the docking scores in HDOCK. The top 10 score docked TLR3/4-SARSV complexes for each construct were assessed.

2.15. Molecular dynamic simulation

A computer technique called molecular dynamic simulation (MDS) is used to examine atomic motions and molecules physically. Chemical physics, material science, and biophysics are all fields where this approach is used [56]. To simulate the molecular dynamics, we used Groningen Machine for Chemical Simulations (GROMACS) that is the fastest software in this benchmark [57]. In addition, the TLR3-vaccine and TLR4-vaccine complexes were simulated using the GROMACS and visualization tools such as VMD. The TLR3/4-vaccine complex is recentered in a triclinic box. Typically, the box margins should be at least 1 nm away from the edges. To fully wrap the protein and avoid unfolding during the MD simulation, this was raised following visual examination using VMD software. The finished box measured for SARSV-TLR3 and SARSV-TLR4 ($12.951 \times 14.632 \times 12.741$ nm^3, $16.017 \times 10.884 \times 10.838$ nm^3). After that, TIP3P water model was used to fill the MD 3D environment. To further neutralize the system and get the concentration to 150 mM, Na^+ and Cl^- ions were added. Steepest descent method was used to energy minimize the simulation box ingredients until it converged at a goal of F_{max} 1000 kJ mol^{-1} nm^{-1}. The covalent bonds were subjected to the restrictions using the Linear Constraint Solver (LINCS) as a way to create the stable bond lengths. For the long-range electrostatics interactions, Particle Mesh Ewald (PME) was also applied. Periodic boundary conditions (PBC) through the XYZ coordinates were used to stop elements from moving outside the defined region of the simulation box. Next, a two-phase equilibration was conducted using 100 ps of NVT and 100 ps of NPT. At a base pressure of 1

Table 3
SARSV (SARS-Vaccine) multi-epitope amino acid sequence with adjuvant at the N-terminus and TAT at the C-terminus.

Vaccine Name	Adjuvant	Length	Vaccine Ensemble
SARS-CoV Vaccine (SARSV)	50 S ribosomal protein L7/L12	406	MAKLSTDELLKEMTLLELSDFVKKFEETFEVTAAAPVAVAAAGAAPAGAAVEAAEEQSEFDVILEAAGDKKI GVIKVVREIVSGLGLKEAKDLVDGAPKPLLEKVAKEAADEAKAKLEAAGATVTV**EAAAK**AKFVAAWTLKAAA **GGGS**DDSEPVLKGVKLHYT**KK**YGDCLGGISARD**KK**SETKCTLKSLSV**KK**LVNSQCDLTGRT**KK** LLTIHRGDPMPN**KK**GGISARDLICAQ**KK**GDCLGGISARDL**KK**ALVNSQCDLTGR**GGGS**CYGVSATK**AAY** KCYGVSATKL**AAY**NYNYKYRYLR**AAY**SLIDLQELGKYEQYIKW**AAY**HNYKYRYL**GGGS**RPFERDISNVPFS **AAY**KGNYNYKYRYLRHGKL**AAY**NYNYKYRYLR**AAY**CYGVSATKL**GGGS**TGALLAAGAAA

bar at 310 K, the Brendsen pressure coupling method was used. Lastly, a 200-ns production MD run was executed. To more precisely gauge the development of the vaccine-TLR3/4 system, UCSF Chimera visualized the MD run. A computer with Apple MacBook pro (M1 Pro 2021), and GROMACS (2023 version) Package used for simulation. The analyzed of the MD trajectory we used the Root mean square deviation (RMSD), Root mean square fluctuation (RMSF), Radius of gyration (Rg), SASA (Solvent accessible surface area), and H-bond (Hydrogen bond).

2.16. Computational cloning and mRNA secondary structure forecasting

Codon optimization was performed in the Java Codon Adaptation Tool following making adjustments the codon use in *Escherichia coli* strain K12 (E. coli, a prokaryotic organism) (JCat) [58]. To increase the efficacy of vaccine expression, E. coli strain K12 was used. Efficiency of the protein's expression was evaluated using the codon optimization index (CAI) and the output sequence's percent GC content. The multi-epitope vaccine codon sequence was modified to include *Xho*I and *Sac*I cleavage sites at the N/C-termini. Using SnapGene software (https://www.snapgene.com), the multi-epitope vaccine was cloned. The optimized SARS vaccine sequence was added separating *Xho*I and *Sac*I restriction enzyme positions in pET28a (+) plasmid. Prediction of the gel agarose was performed to display the clone. Finally, through an optimized cDNA sequence, mfold (http://www.unafold.org/mfold/applications/rna-folding-form.php) ascertained the optimal free energy for mRNA secondary structure.

2.17. Immunological simulation

The C-ImmSim tools was utilized to implement immunological simulation computation with a view to ascertain how the multi-epitope vaccine will affect the host's immunity [59]. We used C-ImmSim (http://kraken.iac.rm.cnr.it/C-IMMSIM/index.php) for this purpose, which simulates three anatomical sections within the body: the lymphatic, bone marrow, and thymus tissue [60]. Moreover, the immune system was simulated using three vaccination injections at time steps of 1, 80, and 180 (0, 26, 60 days). Each time step lasts around 8 h. The total number of simulation steps was 1050 (about a year, 350 days), while the rest of simulation settings were default.

2.18. Binding free energy estimation

The calculation of binding free energy was executed by using functional energy methodologies known as MM-GBSA (Molecular Mechanics-Generalized Born Surface Area), that were run on the Hawkdock web tool [61]. So as to figure out the binding free energy, which comprises van der wall energy, electrostatic energy, polar solvation free energy, solvation free energy, and overall energy. To compute the binding free energy, we retrieved a snapshot every 20ns throughout the MD simulation and then estimated the binding free energy. Lower (negative) binding energies are more favorable at the level of residue. Moreover, the binding free energy binding of TLR3/4-SARSV was foreshowed using the following general formula [62]:

$$\Delta G_{Binding} = \Delta G_{TLR3/4\text{-}SARSV} - (\Delta G_{TLR3/4} + \Delta G_{SARSV})$$

3. Results

3.1. Validation of experimental SARS-CoV epitopes

IEDB yielded 486 experimental epitopes, comprising 34 MHC I, 40 MHC II, and 412 B-lymphocyte epitopes. These epitopes were confirmed using multiple approaches, which are described below, in order to choose the final candidate epitopes for a SARS chimeric vaccine.

3.2. Assessment of immune parameters and solubility of epitopes

In terms of antigenicity, allergenicity, and toxicity, 486 epitopes were evaluated. They were filtered by these analyses, removing 81 B-cell, 11 MHC I, and 4 MHC II epitopes. For selecting B-lymphocytes epitopes, we employed an antigenicity rank score of between 0.9 and 1.7. Eight epitopes exhibited high water solubility according to the solubility prediction, thus five MHC I and four MHC II were obtained to create a SARS multi-epitope vaccine. Altogether 17 epitopes were selected in this step. Then the virulence score was between 1.05 and 1.11, next analyzed the IL-10 in MHC I epitopes that showed most of them were simulated the production of IL-10, and also the analysis of the IFNγ in MHC II demonstrated, the epitopes can simulate the IFNγ (Table 1).

3.3. Valuation of conservancy and human-SARS-CoV-2 homology of epitopes

Using a supply of spike protein from Reference Sequence P59594, all 17 chosen epitopes displayed 100 % sequence conservation with SARS-CoV. According to the findings of the BLASTp homology evaluation, all of the epitopes shared similarity with SARS-CoV-2 and the conserved region showed even if they did not exactly match *Homo sapiens* proteins (identity 70 %). This suggests that a vaccination may be able to effect SARS-CoV-2. The examination of BLASTp demonstrated a several of selected epitopes have a homology with ancestral of coronavirus that this study is based on producing multi-epitope vaccine from ancestral coronavirus preventing the future viruses, whatever we used SARS-CoV that have a 79 % homology with SARS-CoV-2. That can be efficient in some kind of the variants PANGO lineage in SARS-CoV-2 such as AY.113, B.1.617.2, AY.20, AY.3, AY.36, BA.2.12.1, BA.1.1, BA.5.6, BA.4.6, B.6, B.1.1.284, B.1, B.1.1.284, AY.44, AY.26, B, BA.1.

3.4. Analysis of conserved region of SARS-CoV/SARS-CoV-2

The 17 collection sequences consist of SARS-CoV-2 variant and SARS-CoV aligned with MUSCLE algorithm and the conserved regions listed in Table S1. The phylogenetic tree demonstrated in Fig. S1 indicates the relation of spike protein in the different variants and other spices.

3.5. Assessment of physico-chemical properties for epitopes

The majority of the shortlist epitopes had high aliphatic index values

Table 4
Physico-chemical properties of SARS vaccine.

Property	Measurement
SOLpro	0.9049 (Soluble)
Protein-Sol	0.549
Molecular weight	43517.95 Da
Formula	$C_{1945}H_{3104}N_{528}O_{578}S_{12}$
Theoretical pI	9.34 (Basic)
Ext. coefficient	54,710M^{-1} cm^{-1}
Instability index	21.95(Stable)
Aliphatic index	82.86 (Thermostable)
Half-Life	30 h (mammalian reticulocytes, *in vitro*). Over 20 h (yeast, preclinical). Over 10 h (Escherichia coli, preclinical).
Antigenicity	ANTIGENpro (0.7114), VexiJen v2.0 (0.7395) Antigenic
Toxicity	Non-Toxin
Allergenicity	Non-Allergen
GRAVY	−0.260 (Hydrophilic)

(thermostable) and instability index values was ranged −9.98 to 68.49 that indicated to design stable vaccine. Selected epitopes range in molecular weight from 941.11 to 2126.44 Da, and their half-lives in mammalian cells range from 1 to 30 h (Table 1).

3.6. Analysis of population coverage and identifying the MHC alleles relation

IEDB tool was implement to anticipate the coverage of SARSV in human population for the mentioned MHC-I/-II epitopes by estimating the global population coverage. Reference alleles and these epitopes interact. MHC I and II had a 100 % coverage of the global population, with an overall HLA hit of 6.02 and a pc90 mean of 4.32 (Fig. 2). According to an analysis for population coverage of different areas in the world, Europe and North America had the highest coverage, with 100 %, followed by East Africa (91.61 %), North Africa (92.37 %), West Africa (90.87 %), South America (94.01 %), and countries like Iran (91.12 %), China (96.29 %), India (97.49 %), Israel (89.81 %), and Japan (96.33 %). Among 17 epitopes HNYKYRYL has the highest coverage In MHC I (73.35 %) and all of the MHC II epitopes have 100 % coverage (Table 2).

We applied MHCcluster v2.0 tool for testing the interaction between the epitopes chosen from the structural vaccine construct and the MHC I/II alleles. All reference alleles utilized in the population coverage were considered for this analysis (Fig. 3). This figure shows the cluster evaluation for MHC I/II alleles and the demonstration of advanced tree map of MHC I/II. The heatmap's red zone revealed a good interaction among the clustered HLA alleles, but the yellow and orange regions showed a weaker reaction.

3.7. Engineering of chimeric vaccine

The chimeric protein was engineered consisting of 8 B-cells and 9 MHC-I/-II which employed special connectors called "linkers" to attach the HTL, CTL, and B-lymphocytes epitopes. AAY sequence connects CTL and HTL epitopes, while the KK linker interlinks B-cell epitopes. We employed the 50 S ribosomal L7/L12 adjuvant and utilized EAAAK sequence to tailor the adjuvant to PADRE, as well as at the C-Terminal connected TAT sequence, and each sequence (HTL, CTL, B-cell) was connected by GGGS connector sequence (Table 3). This is an overview of construct of our SARS-CoV/SARS-CoV-2 vaccine: Adjuvant-EAAAK-PADRE-BCL-GGGS-CTL-GGGS-HTL-GGGS-TAT.

Table 5
Validation of 3D structure of SARSV with z-score, Ramachandran plot an ERRAT.

SARS Vaccine	Before	After
Validation		
Ramachandran plot details		
Most Favored regions	92.1 %	93.2 %
Additional allowed regions	6.8 %	5.6 %
Generously allowed regions	0.3 %	0.3 %
Disallowed regions	0.8 %	0.8 %
ProSA-web		
Z-score	−4.91	−5.13
ERRAT	88.35	90.42

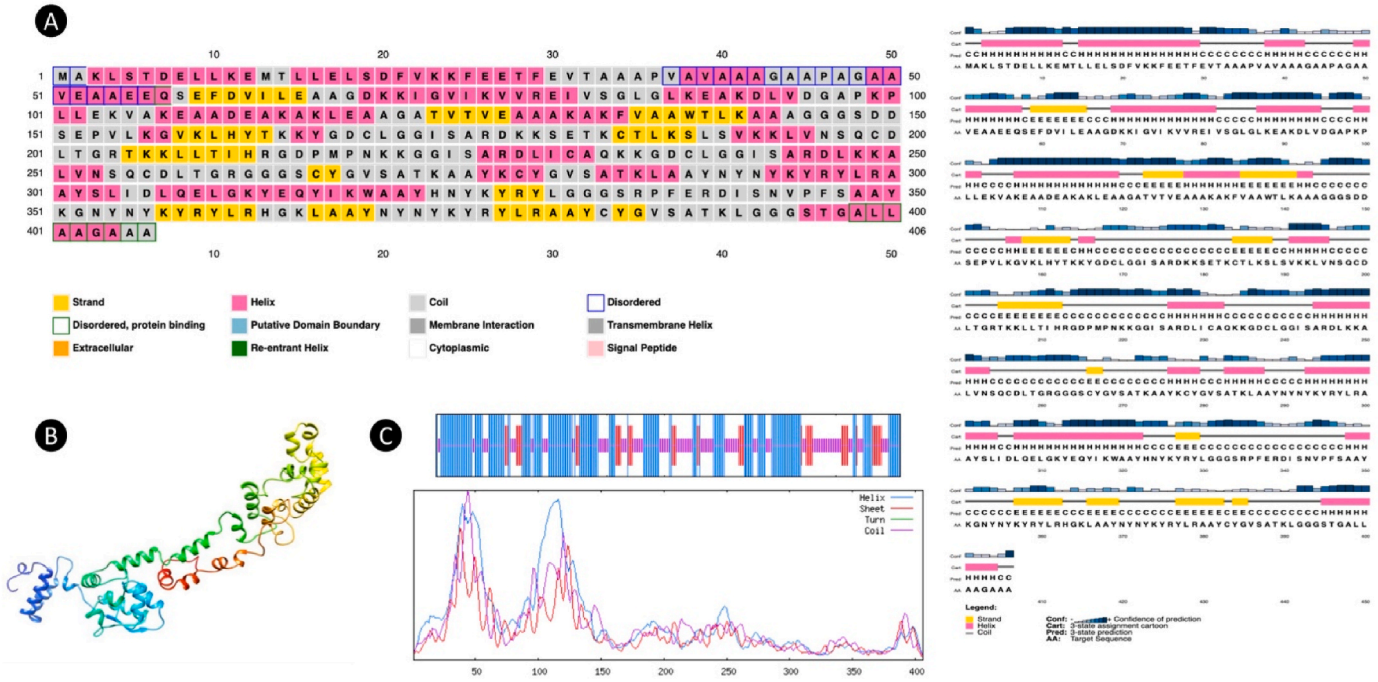

Fig. 4. Structural analysis **A**: Prediction of secondary structure with disorder region in PSIPRED web server **B**: The vaccine's final 3D modeled structure **C**: Frequency of Secondary structure plot detail of alpha helix, Beta sheet, and super coil in SOPMA server.

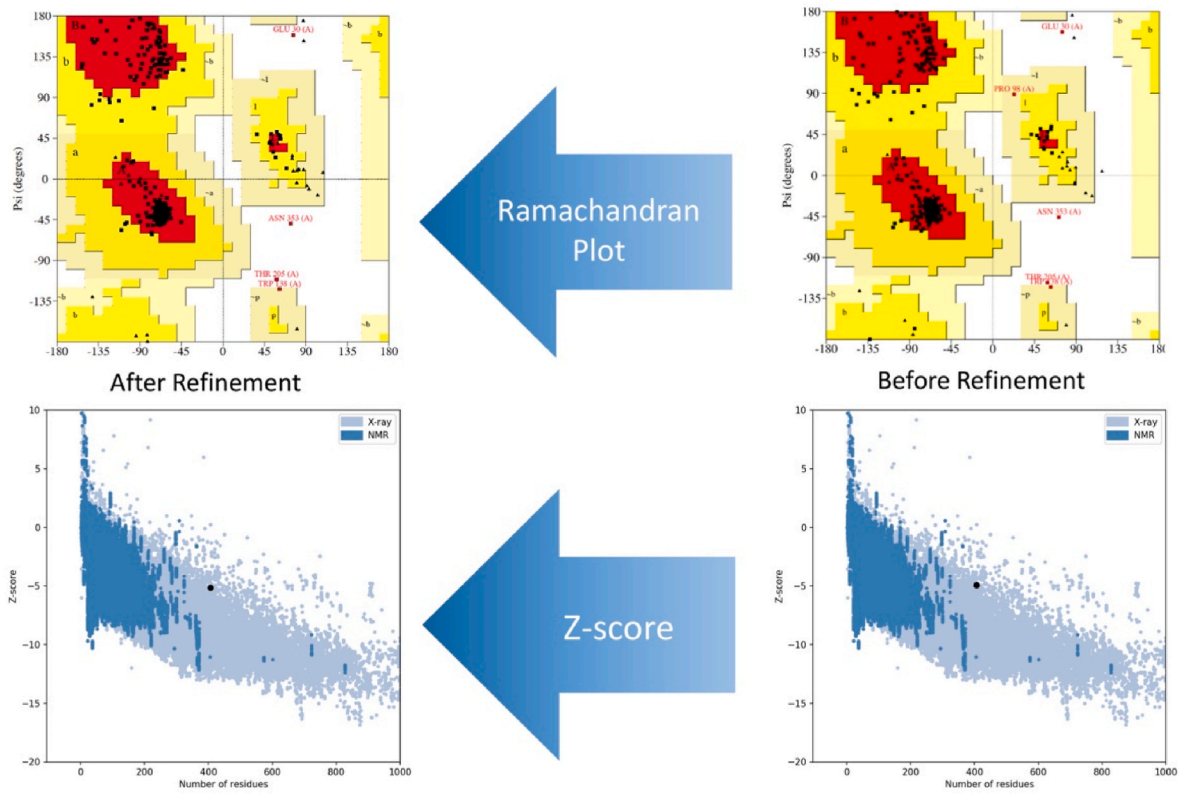

Fig. 5. Validation of tertiary structure of SARSV. Variation of tertiary structure before refinement and after refinement with Z-score in ProSA-web server.

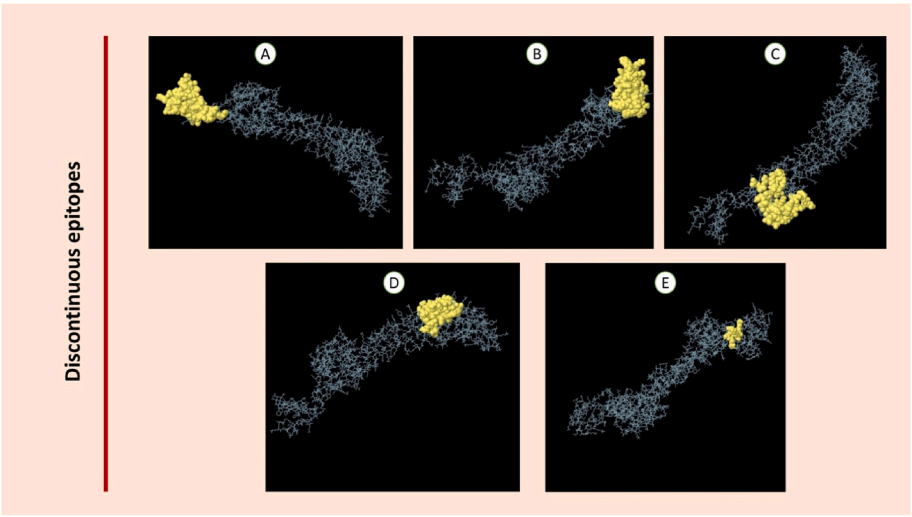

Fig. 6. conformational B-cell epitopes predicted in SARSV. The yellow mark showing conformational epitopes. **A**: 52 residues score: 0.84, **B**: 65 residues score: 0.74, **C**: 52 residues score: 0.63, **D**: 32 residues score: 0.61, **E**: 4 residues score 0.51. (For interpretation of the references to color in this figure legend, the reader is referred to the Web version of this article.)

3.8. Prediction of proteasome cleavage

The analysis of the proteasome cleavage was employed via PCPS server that cleavage position demonstrated in Supplementary material. The score of the prediction of CTL and HTL epitopes from vaccine sequence is significant that confirmed the epitopes for presenting to the T-cell via MHC I/II molecules.

3.9. Evolution of antigenicity, allergenicity, and toxicity of constructed multi-epitope vaccine

The SARSV's antigenicity was predicted by the VaxiJen v2.0 server, which indicated that it was a potential antigen with a 0.71 score, as well as by the ANTIGENpro server, which determined it to be a reasonable antigen with a 0.73 score. Moreover, the AllerTop and ToxinPred tests were utilized to identify allergenicity and toxicity, respectively, and the results demonstrated that the multi-epitope vaccine is non-toxin and non-allergen (Table 4).

Table 6
Linear B-Cell epitope in constructed vaccine by Bcepred.

Prediction parameter	Epitope sequence
Hydrophilicity	EAAEEQSEFD, EAAGDKK, AKEAADEAKAK, AAGGGSDDSEPV, TKKYGDC, SARDKKSETKCT, CAQKKGDC, TGRGGGSC, GGGSTGA
Flexibility	KAAAGGGSDDS, GGISARDKKSETK, CDLTGRTK, DPMPNKKGG, LICAQKKG, CDLTGRGGG, YRYLGGGS, SATKLGGGS
Accessibility	AKLSTDELLKE, FVKKDEETFE, EAAEEQSEFD, EAAGDKK, GLKEAKDLV, PKPLLEKVAKEAADEAKAKLE, GSDDSEPV, VKLHYTKKYGDC, ISARDKKSETKCTLKSLSVKKLVNSQ, DLTGRTKKLLT, HRGDPMPNKKGI, CAQKKGDC, SARDLKKAL, ATKAAYK, AAYNYNYKYRYLRAAY, QELGKYEQYIKWAAYHNYKYRYLGGGSRPFERDISN, AYKGNYNYKYRYLRHGK, AAYNYNYKYRYLRAAY
Exposed Surface	VKKFEET, PKPLLEK, KLHYTKKYGD, ISARDKKSETKC, KSLSVKKLVNSQ, DPMPNKKG, SARDLKK, YNYNYKYRYLR, KYEQYIK, YHNYKYRYL, KGNYNYKYRYLRH, YNYNYNYKYRYLR
Polarity	TDELLKEMTLLE, DFVKKFEETFEVT, VEAAEEQSEFD, EAAGDKK, GLKEAKDLVD, PKPLLEKVAKEAADEAKAKLE, KGVKLHYTKKYG, ISARDKKSETKCTLKSLSVKK, LTGRTKKLLTIHR, SARDLKKAL, YKYRYLRA, QELGKYEQYIK, YHNYKYRY, GSRPFERDI, YKYRYKRHGKLAA, YKYRYLRA
Antigenic Property	LELSDFV, SEFDVIL, KIGVIKVVREIVSGLGL, KPLLEKV, EPVLKGVKLHYTK, KCTLKSLSVKKLVNSQCDL, LVNSQCDL, GSCYGVS, YKCYGVS, YSLIDLQEL

3.10. Evaluation of solubility and physico-chemical characterization of the SARS vaccine constructs

Forecasting solubility through Protein-Sol and the SOLpro service suggested that multi-epitope SARSV has good solublity. SARSV has a molecular weight of 43517.95 Da and a calculated pI of 9.34. (Basic). The Molecular weight is suitable for a desirable inoculation. The *in silico* ramification of the instability index is 21.95, showing good stability, as the stability index was found to be below 40. The aliphatic index of the SARSV was 82.86, indicating that the multi-epitope vaccine is stable. The estimated half-time in mammalian cells is 30 h *in vitro* and 10 h in *E. coli*. The GRAVY value of the constructed is −0.26, indicating that our vaccine is mildly hydrophile. Results of comprehensive physico-chemical properties analysis can be found in Table 4.

3.11. Determining of secondary multi-epitope vaccine structure, tertiary structure, enhancement, and verification

Secondary structural of SARSV using SOPMA and PSIPRED revealed that the multi-epitope construct had 51.48 % -helix, 13.05 % -sheets, and 35,47 % random coil (Fig. 4A–C). By GalaxyTMB, the tertiary structure was created, and the top candidate with the highest quality and score was picked. Galaxyrefine was then carried out to refine the structure of SARSV to improve overall structure. In Table 5, ProsA-web, ERRAT, and Ramachandran plots were applied to verify the modality of the 3D structure. The tertiary construct of the SARSV was enhanced, and model 3 was selected as the top candidate model (Table S2) and the revised 3D structure of the model is shown in Fig. 4B. The Z-score in the initial construct of the model before refinement was −4.91, after refining improved to −5.13 and the analysis of the most favored region before refinement returned a score of 92.1 % for PROCHECK which, after refinement, was improved to 93.2 % (Fig. 5). The ERRAT score was 88.35 and after refining improved to about 90.42 and other detailed information including favorable, generously permitted, and prohibited areas detected in Table 5.

3.12. Prediction of multi-epitope protein unstructured/disorder regions

The ramification from DisEMBL tool (default parameters) discovered the disordered ranges by loops/coil at 41–49, 86–100, 142–157, 165–187, 209–226, 234–243, 256–272, 327–358, and 386–396, by hot-loops description 1–13, 66–74, 84–98, 143–154, 167–224, 256–267 and discorded by Remark-465 definition 42–57, 108–119, 143–151. Finally, the plot for disordered regions can be found in the supplementary material. Furthermore, the possibility of disordered regions was also predicted in PSIPRED (Fig. S2).

3.13. Prediction discontinuous, continuous, and physico-chemical linear B-cell epitopes

SARSV refined 3D structure was utilized to anticipate conformational B-cell epitopes. Ellipro tool discovered 5 discontinuous epitopes consisting of 65, 52, 52, 32, and 4 residues with scores reaching from 0.84 to 0.51 (Table S3). The discontinuous epitopes have been

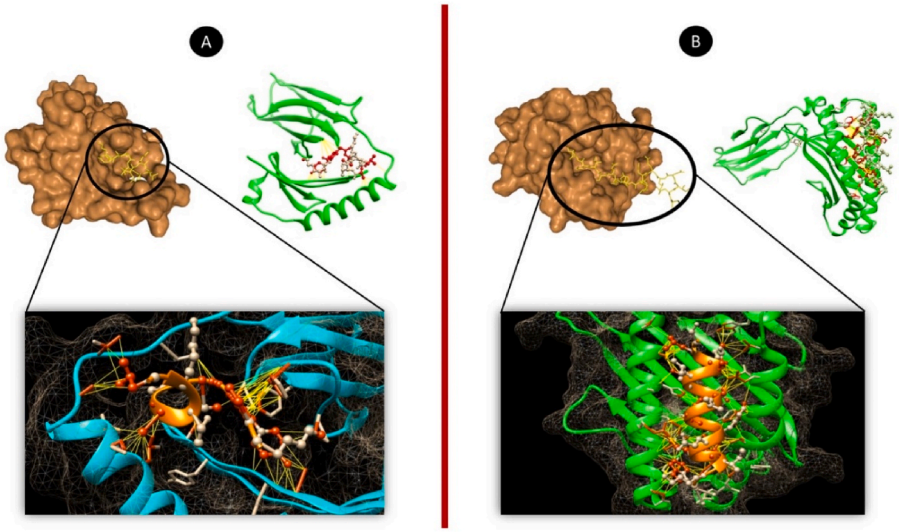

Fig. 7. Docking between peptide and MHC molecules that viewed with UCSF Chimera. **A**: The interaction of MHC II (HLA-DRB*0101) and KCYGVSA. **B**: The interaction of MHC I (HLA-A*0201) and SLIDLQELGKYEQYIKW peptide. The Yellow line showed the interaction of MHC and peptide. (For interpretation of the references to color in this figure legend, the reader is referred to the Web version of this article.)

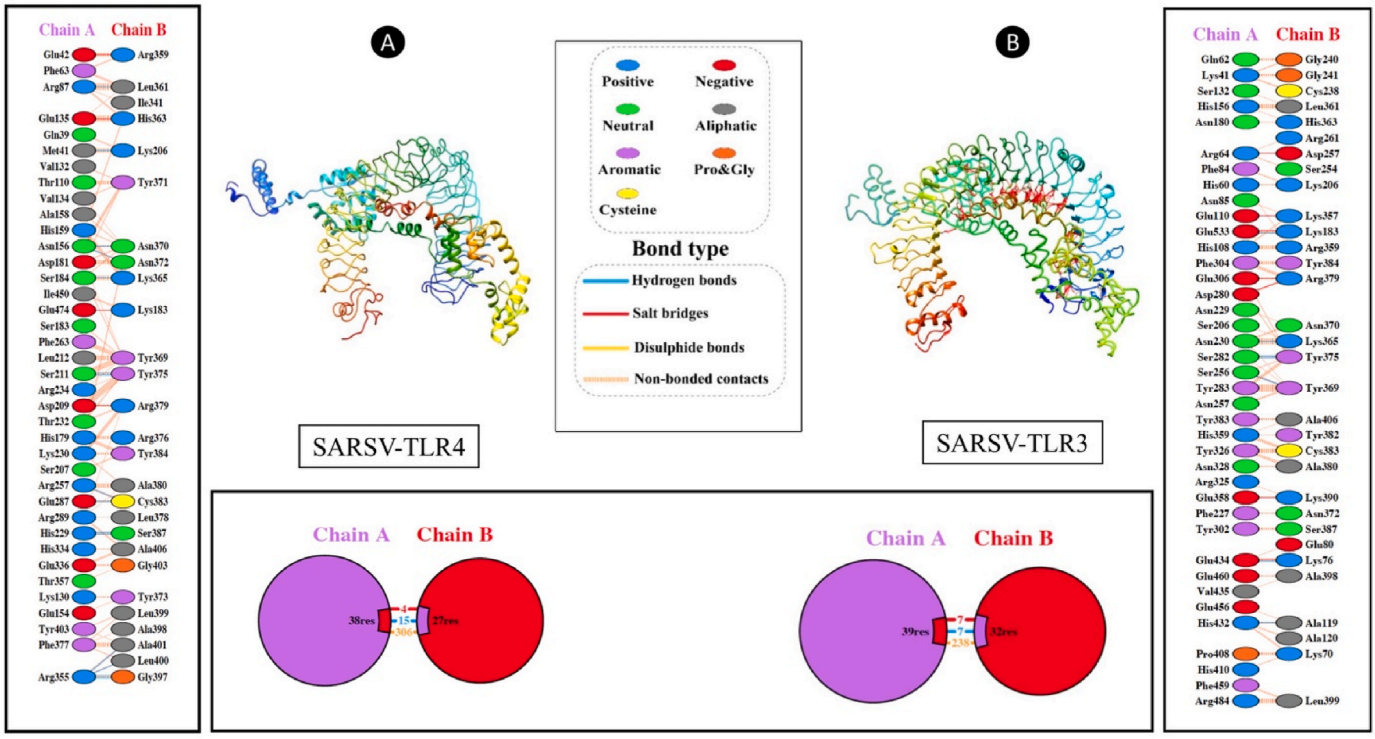

Fig. 8. TLR3/4-Vaccine docking. **A**: The top and high score SARS vaccine construction binding pose with Toll-like receptor-4. The docked complex revealed the contact interaction and the residues in different colors, as well as the hydrogen bonds in blue and other reports. **B**: The top Binding pose of SARS vaccine (SARSV) construct with Toll-like receptor-3. The docked complex (protein-protein) shown the contact interaction. (For interpretation of the references to color in this figure legend, the reader is referred to the Web version of this article.)

demonstrated in Fig. 6 and the linear epitopes indicated in Table 6 with various parameters. The parameters include the Hydrophobicity, Flexibility, Accessibility, Exposed surface, Turn, Polarity, and Antigenic.

3.14. Molecular docking, peptide-MHC, and TLR3/4-SARSV

The final corresponding CTL/HTL epitopes (SLIDLQELGKYEQYIKW, KCYGVSA) were modeled and docked with MHC-I (HLA-A*0201) and MHC II (HLA-DRB1*0101), and the binding was shown to be stable. Energy of binding for the CTL epitope and MHC-I was about −10.2 kcal/mol and MHC II-HTL epitope binding affinity was −8.7 kcal/mol demonstrated in Fig. 7. The orientation of two components in each docking was seen clearly. In Table S4 shows the dissociation constant (Kd), the fraction of charged and polar amino acids on their non-interacting surfaces, and the interaction between the epitopes and the MHC I/II molecules. The molecular docking between the modeled vaccine and TLRs (TLR3/4) was performed using the HDock tool to detect the probable interactions in the TLR-vaccine system. Docking analyses showed the top 10 poses with different scores, we selected the highest ranking. To detect the interactions in the TLR3/4-vaccine complexes, consisting of the hydrogen bonds, salt bridges, along with non-bonded contacts, PDBsum was performed (Fig. 8) The docking score and confidence score of the TLR3/TLR4-vaccine complex were −390.73 and 0.99 and then in TLR4-vaccine were −324.80 and 0.97. The list of Contact between TLR3/4-SARSV in Supplementary data. As shown in Fig. 8, there are 7 salt bridges, 7 hydrogen bonds, and 238 non-bonded contacts in the TLR3-vaccine complex, while the TLR4-vaccine complex has 4 salt bridges, 15 H-bonds, and 306 contacts without bonds.

3.15. Molecular dynamic simulation

MDS was performed using the GROMACS package to obtain the molecular details. We employed the VMD to help the MD data by displaying the recovered frames from the MD xtc/trr output. We built a simulation box that included the TLR3/4-vaccine complex, Na+/Cl-ions with blood-like osmolarity, and utilized the solvent (TIP3P water model). In silico atoms were surrounded by a virtual PBC triclinic box. Contents did not spread beyond the box limitations. The F_{max} of the SARSV-TLR3/4 complex was reduced to 1000 kJ mol^{-1} nm^{-1} (SARSV-TLR3 Highest force: 9.516e+2; norm of force: 9.059e+0, SARSV-TLR4 Maximum force: 9.0137e+2; norm of force: 1.0241075e). After 2920 and 2468 minimization steps, the average potential energy of SARSV-TLR3/4 was determined to be −4.30e+6, −3.36e+6, respectively (Fig. 9A). At 10 ps, NVT stabilization established a steady temperature in both complexes. After 20 ps of NPT equilibration, the pressure and density measurements were steady (Fig. 9B, C, D). During a 200 nano second production MD run, the stabilized systems were allowed to develop. Moreover, the Root mean square deviation (RMSD) of the SARSV-TLR3/4 was steady from the 60ns timepoint, as shown in Fig. 9E. The comparison of the SARSV-TLR3/4 complex RMSD showed the both of them are stable in MD system and the low fluctuation was observed in both complexes. The radius of gyration (Rg) information supplied the compactness of complexes, which revealed their nature. As indicated in Fig. 9F, SARSV-TLR3 compactness increased from 0 to 50ns and then decreased when compared to SARSV-TLR4. Considering that the SARSV-TLR4 decreased during the MD simulation, which demonstrated the compactness of complex. The fluctuation of amino acid residues was calculated via Root mean square deviation (RMSF) that demonstrated in Fig. 9G, consist of TLR3/4 and vaccine in their own complex. Most residues have low fluctuations (less than 1.5 nm) and few residues have large changes. With the goal to identify the alteration in protein volume, the solvent-accession surface area (SASA) for two complexes was examined (Fig. 9H). In comparison to SARSV-TLR4, which has an average SASA value of roughly 481.97, SARSV-TLR3 was found to have a value of 507.74. During a 200ns MD simulation, the complex's volume reduced. Furthermore, the amount of hydrogen bonds and their

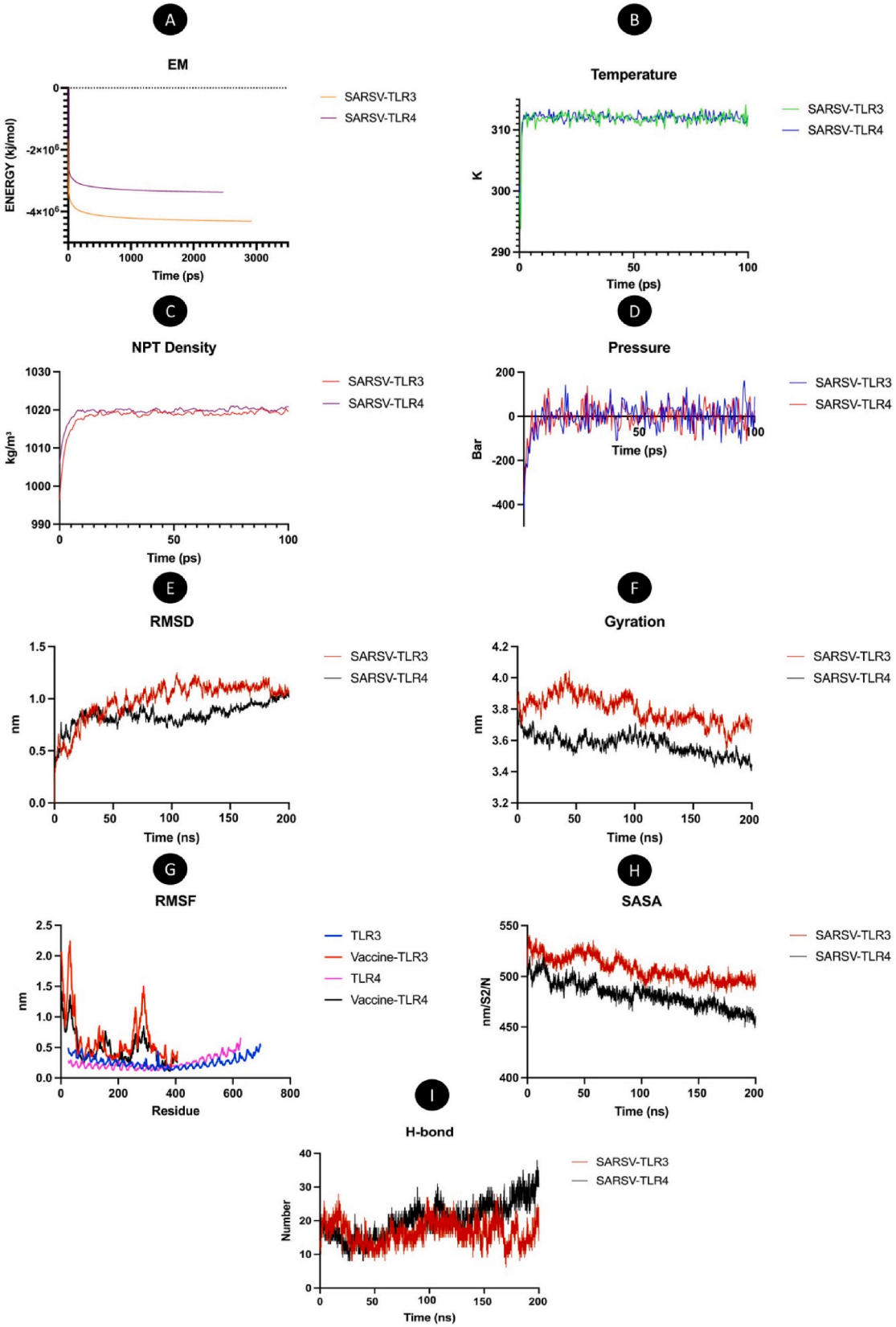

Fig. 9. Molecular Dynamic simulation of TLR3/4-vaccine complex. Result of different simulation step are demonstrated, including **A:** Energy during minimization **B:** Temperature **C:** Density during the NPT equilibration **D:** Pressure **E:** RMSD plot of the c-alpha atoms **F:** Gyration **G:** RMSF to detect the stability of complex during the simulation. **H:** SASA **I:** H-bond.

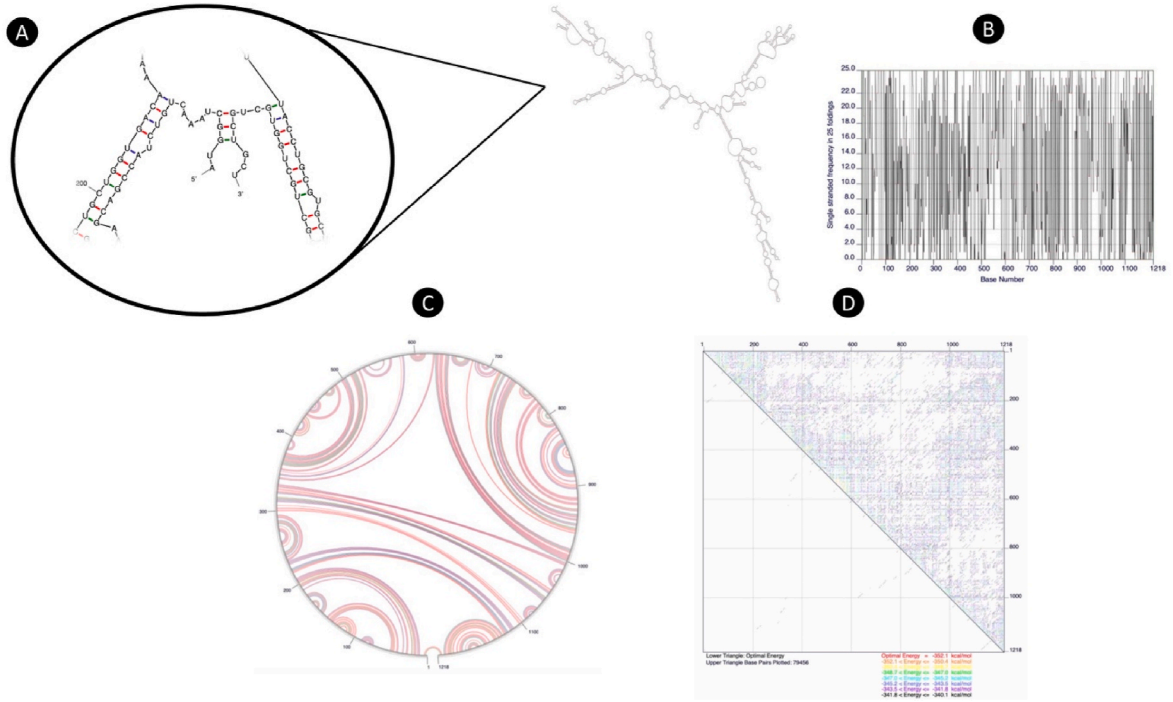

Fig. 10. Design of SARSV mRNA. **A**: Secondary structure of the predicted mRNA, highlighting the 3′ and 5′ terminal that had not hairpin; **B**: Frequency of single stranded strands in 25 folding; **C**: The circular plot displays the RNA construct's base pairs; **D**: The suggested mRNA's energy dot plot.

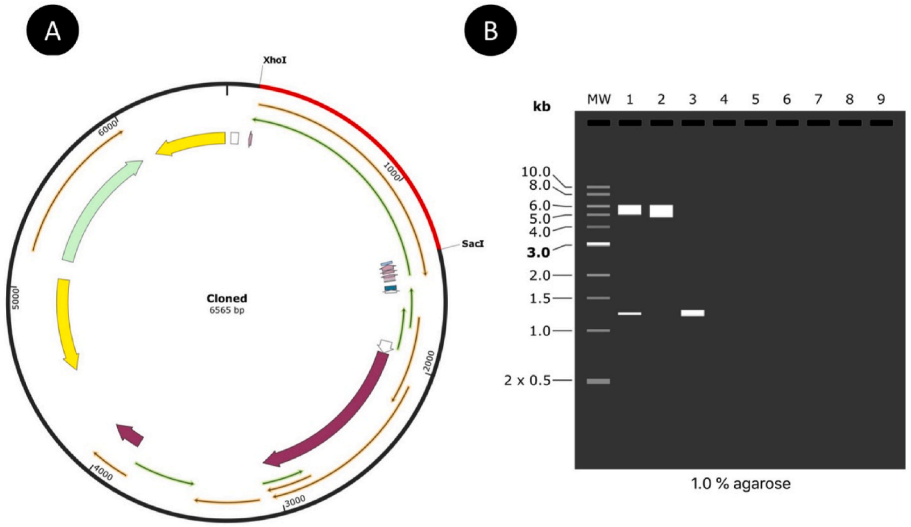

Fig. 11. Cloning and gel simulation **A**: In silico cloning of SARSV construct in pET-28a (+) expression vector where the red sequence cloned. **B**: A vaccine construct built using double separation has been virtual cloned. Line 1: Separated structure of vaccine (SARSV and plasmid) with two enzymes *Xho*I and *Sac*I; line 2: Separation of two enzymes, plasmid pET-28a (+); line 3: digestion of two enzymes. (For interpretation of the references to color in this figure legend, the reader is referred to the Web version of this article.)

formation in MD simulation were employed to explain the SARSV-TLR3/4 stiffness. The average number of hydrogen bonds between SARSV and TLR3 was approximately 16, whereas SARSV and TLR4 had around 20, indicating a stable binding (Fig. 9I).

3.16. Codon optimization and forecasting of mRNA structure

SARSV constructions have 1218 nucleotides in their DNA sequence following reverse translation and codon optimization. In addition, the codon adaptation index (CAI) of SARSV is 1 in the greatest adaptability for E. Coli usage (Fig. S3). Furthermore, the GC-content of the optimized codon was 48.85 % having high expression in the E. coli (strain K12) system. The mRNA secondary structure was forecasted with an unafold server showed the Least energy of the secondary structure of SARSV about −307.38 kcal/mol (initially −357.40 kcal/mol) as shown in Fig. 10. The prediction of the free energy details of 5' end of SARSV mRNA gathered in Table S5.

3.17. Bioinformatics cloning and in silico gel analysis

Prior to cloning, a side of the multi-epitope constructions DNA sequence needed the addition of the sequence that can cut position of

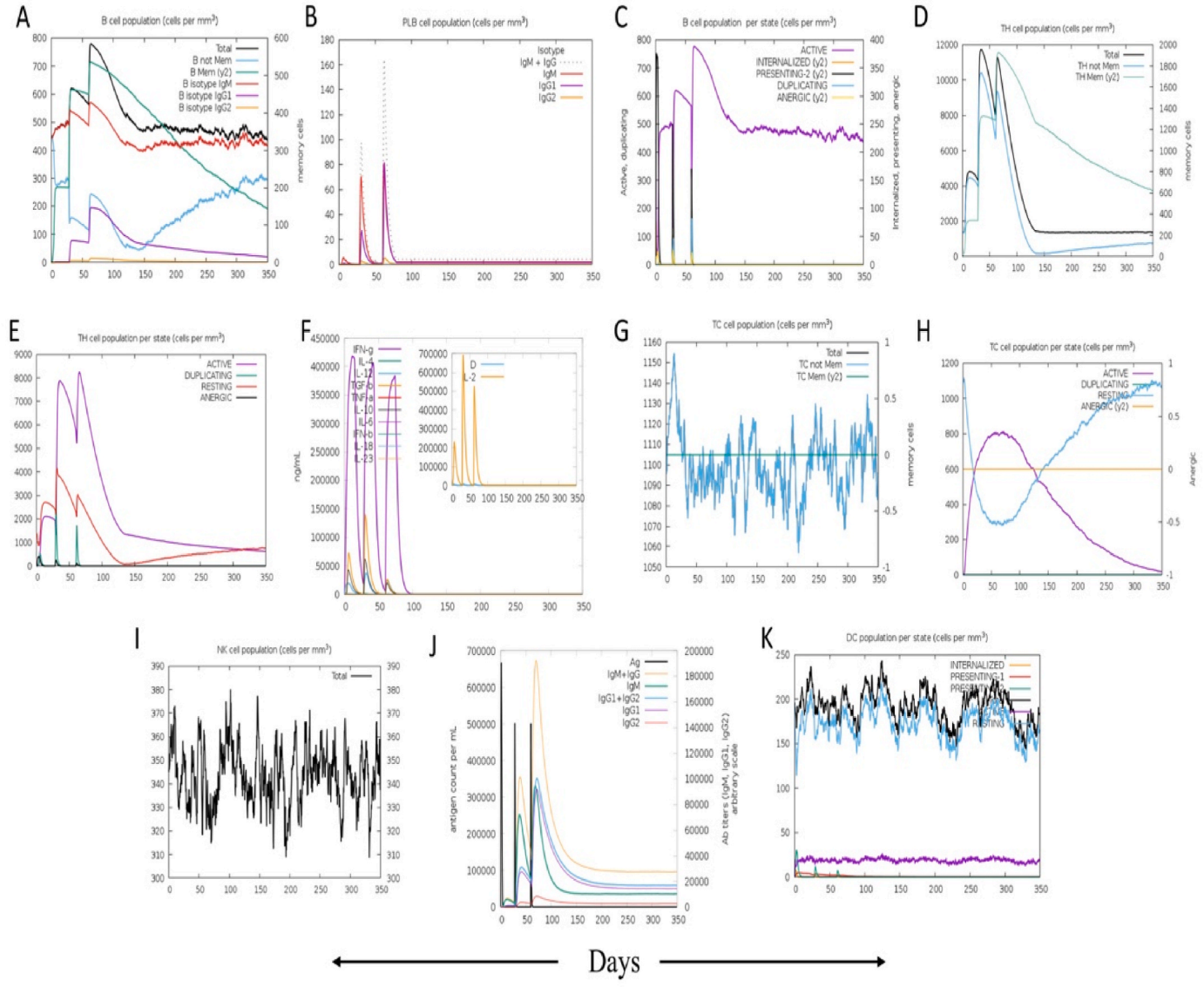

Fig. 12. Immune simulation profile of SARSV that injected 3 doses. **A**: B cell population (cells per mm^3) **B**: PLB cell population IgG/IgM (cells per mm^3) **C**: B cell per state (cells per mm^3) **D**: TH cell population (cells per mm^3) **E**: TH cell population per state (cells per mm^3) **F**: Cytokine profile. **G**: TC cell population (cells per mm^3) **H**: TC cell population per state (cells per mm^3) **I**: NK cell population (cells per mm^3) **J**: Antigen count **K**: DC population per state (cells per mm^3).

Table 7
Using MM/GBSA method for computation of binding free energy in TLR3/4 complex.

Energy Component	MM/GBSA (kcal/mol)	
	SARSV-TLR3 complex	SARSV-TLR4 complex
	Average	Average
vdW	−171.42	−173.82
ELE	−1397.4	−4565.07
GB	1550.82	4664.07
SA	−22.93	−23.31
TOTAL	−40.93	−98.66

*Xho*I and *Sac*I (CTCGAG at the N-ending and GAGCTC at the C-ending). SARSV's new DNA sequence contained 1230 nucleotides (Table S6 and Fig. S4). The nucleotide sequence of the chimeric protein was added to the pET-28a (+) vector after *Xho*I (position 158) and before *Sac*I (position 190) using SnapGene. As shown in Fig. 11A, overall, the cloned plasmid containing the SARSV construct includes 6565bp. After cutting the plasmid with the *Xho*I and *Sac*I enzymes, the virtual agarose gel simulation produced by the SnapGene program demonstrated the existence of the insert alone (Fig. 11B).

3.18. Immune simulation

C-ImmSim was used to simulate the immune system. Fig. 12 provides information on the immunological feedback to injections of the SARSV virus at 1, 80, and 180 days (days 0, 26, and 60). Even as the number of antigens decreased, the immune response's antibody level remained constant. After each injection, antigen levels rose (by over 600,000 upon the first vaccination and 500,000 upon injection with first and second booster dosages). With each injection of the vaccine that exposed the host immune system, the development of secondary immune feedbacks (IgM + IgG: huge titer of over 200000/ml) were observed. At 50 and 100 days the highest level of antibody was reached, >200,000 titer per ml. The initial, secondary, and tertiary immune feedbacks were detected in the form of those with a considerable B-lymphocytes amount and increased levels of IgM, IgG, and other isotypes. After each injection, pre-activation of CTLs and the expansion of active CTLs were seen.

Moreover, the maximal population of HTLs, which demonstrated an adaptive immune response against SARSV, was seen at approximately 10,000–12000 cells per mm3. Moreover, the secondary immune response had the highest level of cytokines, particularly IFN-γ, which peaked over 400,000 ng/ml.

3.19. Estimation of docking free energy by MM/GBSA

The MM/GBSA technique was employed to compute the binding free energy (ΔG) of the SARSV-TLR3/4 complex, and the results are presentedz in Table 7. SARSV-TLR3 and SARSV-TLR4 complexes have total binding free energies of −40.93 and −98.66 kcal/mol, respectively. Energetically strong and stable binding of each complex was corroborated by the high negative ΔG.

4. Discussion

The current COVID-19, which initially presented problems in 2019 in Wuhan, China, mutated and transmitted the dominant variety (sub-lineage of omicron) over the world like the previous dissemination of severe acute respiratory syndrome (SARS) and Middle Eastern respiratory disease (MERS) and therefore, SARS-CoV-2 has demonstrated strong transmissibility [63] and will initiate an uncontrollable outbreak in the future. The Immunoinformatics technique can be used to create and construct a potential microbiome vaccine (Bacteria, parasitic, and viral disease) [64]. Using the structural proteins (spike Protein) of ancestral viruses in coronaviruses, which have high similarity and are also available target proteins, a multi-epitope vaccine (SARSV) was developed in this research [14,65,66]. Prior research indicated that the spike protein was an important point for vaccine evolution [55–57] and are quite effective, we employed the SARS-CoV experimental epitopes from the IEDB antigenic. We have previously designed a vaccine utilizing non-structural proteins and spiker protein of the three majors human CoVs [67]**.** In the present study, we further found that our newly designed vaccine comprising virulent epitopes is an antigen and soluble, but not allergenic or toxic. By comparing all of the selected epitopes, the similarity between SARS-CoV and SARS-CoV-2 variations was determined, and this showed that the ancestral epitope of SARS-CoV-2 can be helpful for developing vaccines and preventing against new and future variants. Using the AAY, KK, GGGS, and EAAAK that linked adjuvant to epitopes that those linkers supplied proteasome cleavage sites for immune cells, the final SARSV structure comprising CTL, HTL, and B-lymphocyte epitopes was made [42]. Also, our adjuvant 50 S ribosomal protein L7/L12 with the N-ending inserted was employed in many experiments [68] shown that may improve immune function, particularly in dendritic cells that supported innate and adaptive immunity and presented antigens, and that 50 S ribosomal protein L7/L12 was identified by TLR4 to drive DC maturation [36]. Moreover, the PADRE sequence was included, which can aid in boosting the antigenicity [37] as demonstrated by *in silico* method. Finally, TAT was added for the enhancement SARSV construct to the C-terminal, which aids in the penetration of several peptides into mammalian cells [69]. The first step in predicting 3D structure was to determine the SARSV construct using the SOPMA and PSIPRED web servers. After this, modeling and tertiary structure refinement were utilized to verify the 3D construct, with the Ramachandran plot, Z-score, and ERRAT analyses demonstrating an adjusted construct. TLR3/4 docking results indicated a potential hydrophilic contact [70]. The immunological simulation had a noticeable response, including humoral and cell-mediated growth of IFN-gamma and other cytokines, immune cells, and antibodies. The MD simulation highlighted that the TLR3/4-vaccine complex was stable during the analysis of RMSD, RMSF, SASA, H-bond, and Rg. Therefore, computing the binding free energy with MM/GBSA showed that the binding was appropriate and effective. Although, during the quick assessment of SARS-CoV-2 variations, vaccination effectiveness frequently dropped [71] and the Omicron BA.4 sub-lineage exhibited good tolerance to neutralizing antibodies [72]. It must examine the newest SARS-CoV-2 vaccine with advanced analysis that can cover the future variants. The advantages of employing this strategy are that it is quicker and less expensive, as demonstrated by the immunoinformatics methods, which are promising means for creating high effectiveness vaccines. The experimental spike protein epitopes from the innovative multi-epitope vaccination for SARS-CoV and SARS-CoV-2 demonstrated the relationship between the experimental spike protein and potential of the ancestral vaccine to anticipate and prevent the new variants. Even so, it was critical to conduct in vivo tests and evaluate the chimeric protein in order to demonstrate the effectiveness of immunoinformatics as well as accelerate the development of the vaccine. Also, ancestral analysis helps us choose the epitope that is most successful at inhibiting viruses, even though we may develop an ancestral vaccine that is effective against viruses that mutate quickly and escape the immune system.

5. Conclusion

As SARS-CoV-2 has the mortally varied S protein, we created an ancestral vaccine using experimental SARS-CoV epitopes which is effective against both familiar coronaviruses (SARS-CoV-2 and SARS-CoV) spike protein. In this investigation, a SARS vaccine that can stimulate humoral and cell-regulated immunological feedbacks were created using immunoinformatic methods. 5 CTL, 4 HTL, and 8 B-lymphocytes epitopes make up the final vaccination after the functional approach and immunoinformatic methods that vaccine included 406 aa. To evaluate the final vaccine's stability and immunological responses, the SARSV underwent analysis, molecular docking with TLR3/4, molecular dynamic modeling, and immune simulation. The results revealed that SARSV can effectively target the spike protein.

CRediT authorship contribution statement

Cena Aram: Writing – review & editing, Writing – original draft, Project administration, Methodology, Investigation, Formal analysis. **Parsa Alijanizadeh:** Conceptualization, Data curation, Methodology, Writing – original draft. **Kiarash Saleki:** Writing – review & editing, Writing – original draft, Validation, Supervision, Data curation, Conceptualization. **Leila Karami:** Writing – review & editing, Writing – original draft, Supervision, Data curation, Conceptualization.

Declaration of competing interest

The authors declare that they have no known competing financial interests or personal relationships that could have appeared to influence the work reported in this paper.

Data availability

Data will be made available on request.

Acknowledgments

We thank the Student Research Committee and USERN Office of Babol University of Medical Sciences.

Appendix A. Supplementary data

Supplementary data to this article can be found online at https://doi.org/10.1016/j.bbrep.2024.101745.

References

[1] M.B. Loeb, Severe Acute Respiratory Syndrome [Internet], WHO, 2006, pp. 465–472. Available from: https://www.who.int/health-topics/severe-acute-respiratory-syndrome#tab=tab_1.

[2] M.D. Sørensen, B. Sørensen, R. Gonzalez-Dosal, C.J. Melchjorsen, J. Weibel, J. Wang, et al., Severe acute respiratory syndrome (SARS): development of diagnostics and antivirals, Ann. N. Y. Acad. Sci. 1067 (1) (2006) 500–505.

[3] R. Lu, X. Zhao, J. Li, P. Niu, B. Yang, H. Wu, et al., Genomic characterisation and epidemiology of 2019 novel coronavirus: implications for virus origins and receptor binding, Lancet (London, England) 395 (10224) (2020 Feb) 565–574.

[4] A. Zeidler, T.M. Karpinski, SARS-CoV, MERS-CoV, SARS-CoV-2 comparison of three emerging coronaviruses [Internet], Jundishapur J. Microbiol. 13 (6) (2020) e103744. Available from: https://brieflands.com/articles/jjm-103744.html.

[5] P. Jha, P.E. Brown, R. Ansumana, Counting the global COVID-19 dead, Lancet (London, England) 399 (2022) 1937–1938. England.

[6] T. Singhal, The emergence of omicron: challenging times are here again, Indian J. Pediatr. 89 (5) (2022 May) 490–496.

[7] X.-Y. Ge, J.-L. Li, X.-L. Yang, A.A. Chmura, G. Zhu, J.H. Epstein, et al., Isolation and characterization of a bat SARS-like coronavirus that uses the ACE2 receptor, Nature 503 (7477) (2013 Nov) 535–538.

[8] K.-S. Yeung, G.A. Yamanaka, N.A. Meanwell, Severe acute respiratory syndrome coronavirus entry into host cells: opportunities for therapeutic intervention, Med. Res. Rev. 26 (4) (2006 Jul) 414–433.

[9] A.R. Fehr, S. Perlman, Coronaviruses: an overview of their replication and pathogenesis [Internet], in: H.J. Maier, E. Bickerton, P. Britton (Eds.), Coronaviruses: Methods and Protocols, Springer New York, New York, NY, 2015, pp. 1–23, https://doi.org/10.1007/978-1-4939-2438-7_1.

[10] J. Cui, F. Li, Z.-L. Shi, Origin and evolution of pathogenic coronaviruses, Nat. Rev. Microbiol. 17 (3) (2019 Mar) 181–192.

[11] Y.-J. Tan, S.G. Lim, W. Hong, Characterization of viral proteins encoded by the SARS-coronavirus genome, Antivir. Res. 65 (2) (2005 Feb) 69–78.

[12] X. Tian, C. Li, A. Huang, S. Xia, S. Lu, Z. Shi, et al., Potent Binding of 2019 Novel Coronavirus Spike Protein by a SARS Coronavirus-specific Human Monoclonal Antibody, vol. 9, Emerging microbes & infections, United States, 2020, pp. 382–385.

[13] Y. Huang, C. Yang, X.-F. Xu, W. Xu, S.-W. Liu, Structural and functional properties of SARS-CoV-2 spike protein: potential antivirus drug development for COVID-19, Acta Pharmacol. Sin. 41 (9) (2020 Sep) 1141–1149.

[14] L. Du, Y. He, Y. Zhou, S. Liu, B.-J. Zheng, S. Jiang, The spike protein of SARS-CoV–a target for vaccine and therapeutic development, Nat. Rev. Microbiol. 7 (3) (2009 Mar) 226–236.

[15] X. Xia, Domains and functions of spike protein in sars-cov-2 in the context of vaccine design, Viruses 13 (1) (2021 Jan).

[16] W.T. Harvey, A.M. Carabelli, B. Jackson, R.K. Gupta, E.C. Thomson, E.M. Harrison, et al., SARS-CoV-2 variants, spike mutations and immune escape, Nat. Rev. Microbiol. 19 (7) (2021 Jul) 409–424.

[17] Y.N. Lamb, BNT162b2 mRNA COVID-19 vaccine: first approval, Drugs 81 (4) (2021 Mar) 495–501.

[18] FDA authorizes Moderna COVID-19 vaccine, Med. Lett. Drugs Ther. 63 (1616) (2021 Jan) 9–10.

[19] A.I. Francis, S. Ghany, T. Gilkes, S. Umakanthan, Review of COVID-19 vaccine subtypes, efficacy and geographical distributions, Postgrad. Med. 98 (1159) (2022 May) 389–394.

[20] A. Awadasseid, Y. Wu, Y. Tanaka, W. Zhang, Current advances in the development of SARS-CoV-2 vaccines, Int. J. Biol. Sci. 17 (1) (2021) 8–19.

[21] R. Sharma, S. Tiwari, A. Dixit, Covaxin: an overview of its immunogenicity and safety trials in India, Bioinformation 17 (10) (2021) 840–845.

[22] Z. Zhang, J. Mateus, C.H. Coelho, J.M. Dan, C.R. Moderbacher, R.I. Gálvez, et al., Humoral and cellular immune memory to four COVID-19 vaccines, Cell 185 (14) (2022 Jul) 2434–2451.e17.

[23] T.T. Le, J.P. Cramer, R. Chen, S. Mayhew, Evolution of the COVID-19 vaccine development landscape [Internet], Nat. Rev. Drug Discov. 19 (10) (2020) 667–668, https://doi.org/10.1038/d41573-020-00151-8.

[24] Ul Qamar M. Tahir, Z. Shokat, I. Muneer, U.A. Ashfaq, H. Javed, F. Anwar, et al., Multiepitope-based subunit vaccine design and evaluation against respiratory syncytial virus using reverse vaccinology approach, Vaccines 8 (2) (2020 Jun).

[25] S. Mahmud, M.O. Rafi, G.K. Paul, M.M. Promi, M.S.S. Shimu, S. Biswas, et al., Designing a multi-epitope vaccine candidate to combat MERS-CoV by employing an immunoinformatics approach [Internet], Sci. Rep. 11 (1) (2021) 15431, https://doi.org/10.1038/s41598-021-92176-1.

[26] U.A. Ashfaq, B. Ahmed, De novo structural modeling and conserved epitopes prediction of Zika virus envelop protein for vaccine development, Viral Immunol. 29 (7) (2016 Sep) 436–443.

[27] B. Ahmad, U.A. Ashfaq, M.-U. Rahman, M.S. Masoud, M.Z. Yousaf, Conserved B and T cell epitopes prediction of ebola virus glycoprotein for vaccine development: an immuno-informatics approach, Microb. Pathog. 132 (2019 Jul) 243–253.

[28] S. Aiman, Y. Alhamhoom, F. Ali, N. Rahman, L. Rastrelli, A. Khan, et al., Multi-epitope chimeric vaccine design against emerging Monkeypox virus via reverse vaccinology techniques- a bioinformatics and immunoinformatics approach [Internet], Front. Immunol. 13 (2022). Available from: https://www.frontiersin.org/articles/10.3389/fimmu.2022.985450.

[29] I.A. Doytchinova, D.R. Flower, VaxiJen: a server for prediction of protective antigens, tumour antigens and subunit vaccines, BMC Bioinf. 8 (2007 Jan) 4.

[30] I. Dimitrov, I. Bangov, D.R. Flower, I. Doytchinova, AllerTOP v.2–a server for in silico prediction of allergens, J. Mol. Model. 20 (6) (2014 Jun) 2278.

[31] S. Gupta, P. Kapoor, K. Chaudhary, A. Gautam, R. Kumar, G.P.S. Raghava, In silico approach for predicting toxicity of peptides and proteins, PLoS One 8 (9) (2013) e73957.

[32] A. Garg, D. Gupta, VirulentPred: a SVM based prediction method for virulent proteins in bacterial pathogens [Internet], BMC Bioinf. 9 (1) (2008) 62, https://doi.org/10.1186/1471-2105-9-62.

[33] S.F. Altschul, W. Gish, W. Miller, E.W. Myers, D.J. Lipman, Basic local alignment search tool, J. Mol. Biol. 215 (3) (1990 Oct) 403–410.

[34] K. Tamura, G. Stecher, S. Kumar, MEGA11: molecular evolutionary genetics analysis version 11, Mol. Biol. Evol. 38 (7) (2021 Jun) 3022–3027.

[35] W. Li, M.D. Joshi, S. Singhania, K.H. Ramsey, A.K. Murthy, Peptide vaccine: progress and challenges, Vaccines 2 (3) (2014 Jul) 515–536.

[36] S.J. Lee, S.J. Shin, M.H. Lee, M.-G. Lee, T.H. Kang, W.S. Park, et al., A potential protein adjuvant derived from Mycobacterium tuberculosis Rv0652 enhances dendritic cells-based tumor immunotherapy, PLoS One 9 (8) (2014) e104351.

[37] A.O. Fadaka, N.R.S. Sibuyi, D.R. Martin, M. Goboza, A. Klein, A.M. Madiehe, et al., Immunoinformatics design of a novel epitope-based vaccine candidate against dengue virus, Sci. Rep. 11 (1) (2021 Oct) 19707.

[38] N. Nezafat, Y. Ghasemi, G. Javadi, M.J. Khoshnoud, E. Omidinia, A novel multi-epitope peptide vaccine against cancer: an in silico approach, J. Theor. Biol. 349 (2014 May) 121–134.

[39] H. Tarrahimofrad, S. Rahimnahal, J. Zamani, E. Jahangirian, S. Aminzadeh, Designing a multi-epitope vaccine to provoke the robust immune response against influenza A H7N9 [Internet], Sci. Rep. 11 (1) (2021) 24485, https://doi.org/10.1038/s41598-021-03932-2.

[40] V.S. Ayyagari, C.V. T, A.P. K, K. Srirama, Design of a multi-epitope-based vaccine targeting M-protein of SARS-CoV2: an immunoinformatics approach, J. Biomol. Struct. Dyn. 40 (7) (2022 Apr) 2963–2977.

[41] R. Arai, H. Ueda, A. Kitayama, N. Kamiya, T. Nagamune, Design of the linkers which effectively separate domains of a bifunctional fusion protein, Protein Eng. 14 (8) (2001 Aug) 529–532.

[42] X. Chen, J.L. Zaro, W.-C. Shen, Fusion protein linkers: property, design and functionality, Adv. Drug Deliv. Rev. 65 (10) (2013 Oct) 1357–1369.

[43] A. Yano, A. Onozuka, Y. Asahi-Ozaki, S. Imai, N. Hanada, Y. Miwa, et al., An ingenious design for peptide vaccines [Internet], Vaccine 23 (17) (2005) 2322–2326. Available from: https://www.sciencedirect.com/science/article/pii/S0264410X05000344.

[44] A.-M. Lennon-Duménil, A.H. Bakker, P. Wolf-Bryant, H.L. Ploegh, C. Lagaudrière-Gesbert, A closer look at proteolysis and MHC-class-II-restricted antigen presentation [Internet], Curr. Opin. Immunol. 14 (1) (2002) 15–21. Available from: https://www.sciencedirect.com/science/article/pii/S095279150100293X.

[45] R. Dong, Z. Chu, F. Yu, Y. Zha, Contriving multi-epitope subunit of vaccine for COVID-19: immunoinformatics approaches, Front. Immunol. 11 (2020) 1784.

[46] M. Gomez-Perosanz, A. Ras-Carmona, P.A. Reche, PCPS: a web server to predict proteasomal cleavage sites, Methods Mol. Biol. 2131 (2020) 399–406.

[47] M. Thomsen, C. Lundegaard, S. Buus, O. Lund, M. Nielsen, MHCcluster, a method for functional clustering of MHC molecules, Immunogenetics 65 (9) (2013 Sep) 655–665.

[48] M. Hebditch, M.A. Carballo-Amador, S. Charonis, R. Curtis, J. Warwicker, Protein-Sol: a web tool for predicting protein solubility from sequence, Bioinformatics 33 (19) (2017 Oct) 3098–3100.

[49] C.N. Magnan, A. Randall, P. Baldi, SOLpro: accurate sequence-based prediction of protein solubility, Bioinformatics 25 (17) (2009 Sep) 2200–2207.

[50] PROCHECK: validation of protein-structure coordinates [Internet], in: International Tables for Crystallography. Willey Online Libr, F Chapter, 2006, pp. 521–525, https://doi.org/10.1107/9780955360206000882.

[51] J. Ponomarenko, H.-H. Bui, W. Li, N. Fusseder, P.E. Bourne, A. Sette, et al., ElliPro: a new structure-based tool for the prediction of antibody epitopes, BMC Bioinf. 9 (2008 Dec) 514.

[52] A. Lamiable, P. Thévenet, J. Rey, M. Vavrusa, P. Derreumaux, P. Tufféry, PEP-FOLD3: faster de novo structure prediction for linear peptides in solution and in complex, Nucleic Acids Res. 44 (W1) (2016 Jul) W449–W454.

[53] L.C. Xue, J.P. Rodrigues, P.L. Kastritis, A.M. Bonvin, A. Vangone, PRODIGY: a web server for predicting the binding affinity of protein-protein complexes, Bioinformatics 32 (23) (2016 Dec) 3676–3678.

[54] Y. Yan, D. Zhang, P. Zhou, B. Li, S.-Y. Huang, HDOCK: a web server for protein-protein and protein-DNA/RNA docking based on a hybrid strategy, Nucleic Acids Res. 45 (W1) (2017 Jul) W365–W373.

[55] R.A. Laskowski, J. Jabłońska, L. Pravda, R.S. Vařeková, J.M. Thornton, PDBsum: structural summaries of PDB entries, Protein Sci. 27 (1) (2018 Jan) 129–134.

[56] L.R. Cao, C.Y. Zhang, D.L. Zhang, H.Y. Chu, Y Bin Zhang, G.H. Li, Recent developments in using molecular dynamics simulation techniques to study biomolecules, Wuli Huaxue Xuebao/Acta Phys. Chim. Sin. 33 (7) (2017) 1354–1365.

[57] D. Van Der Spoel, E. Lindahl, B. Hess, G. Groenhof, A.E. Mark, H.J.C. Berendsen, GROMACS: fast, flexible, and free, J. Comput. Chem. 26 (16) (2005 Dec) 1701–1718.

[58] A. Grote, K. Hiller, M. Scheer, R. Münch, B. Nörtemann, D.C. Hempel, et al., JCat: a novel tool to adapt codon usage of a target gene to its potential expression host, Nucleic Acids Res. 33 (Web Server issue) (2005 Jul) W526–W531.

[59] N. Rapin, O. Lund, M. Bernaschi, F. Castiglione, Computational immunology meets bioinformatics: the use of prediction tools for molecular binding in the simulation of the immune system, PLoS One 5 (4) (2010 Apr) e9862.

[60] N. Rapin, O. Lund, F. Castiglione, Immune system simulation online [Internet], Bioinformatics 27 (14) (2011) 2013–2014, https://doi.org/10.1093/bioinformatics/btr335.

[61] G. Weng, E. Wang, Z. Wang, H. Liu, F. Zhu, D. Li, et al., HawkDock: a web server to predict and analyze the protein–protein complex based on computational docking

and MM/GBSA [Internet], Nucleic Acids Res. 47 (W1) (2019) W322–W330, https://doi.org/10.1093/nar/gkz397.
[62] A. Onufriev, D. Bashford, D.A. Case, Exploring protein native states and large-scale conformational changes with a modified generalized born model, Proteins 55 (2) (2004 May) 383–394.
[63] X. He, W. Hong, X. Pan, G. Lu, X. Wei, SARS-CoV-2 Omicron variant: characteristics and prevention [Internet], MedComm 2 (4) (2021) 838–845. Available from: https://onlinelibrary.wiley.com/doi/abs/10.1002/mco2.110.
[64] R. Kaur, N. Arora, M.A. Jamakhani, S. Malik, P. Kumar, F. Anjum, et al., Development of multi-epitope chimeric vaccine against Taenia solium by exploring its proteome: an in silico approach, Expert Rev. Vaccines 19 (1) (2020 Jan) 105–114.
[65] A. Sternberg, C. Naujokat, Structural features of coronavirus SARS-CoV-2 spike protein: targets for vaccination [Internet], Life Sci. 257 (2020) 118056. Available from: https://www.sciencedirect.com/science/article/pii/S0024320520308079.
[66] Q. Wang, G. Wong, G. Lu, J. Yan, G.F. Gao, MERS-CoV spike protein: targets for vaccines and therapeutics [Internet], Antivir. Res. 133 (2016) 165–177. Available from: https://www.sciencedirect.com/science/article/pii/S0166354216301826.
[67] A. Rahmani, M. Baee, K. Saleki, S. Moradi, H.R. Nouri, Applying high throughput and comprehensive immunoinformatics approaches to design a trivalent subunit vaccine for induction of immune response against emerging human coronaviruses SARS-CoV, MERS-CoV and SARS-CoV-2, J. Biomol. Struct. Dyn. 40 (13) (2022 Aug) 6097–6113.
[68] M. Tahir ul Qamar, S. Ahmad, I. Fatima, F. Ahmad, F. Shahid, A. Naz, et al., Designing multi-epitope vaccine against Staphylococcus aureus by employing subtractive proteomics, reverse vaccinology and immuno-informatics approaches [Internet], Comput. Biol. Med. 132 (2021) 104389. Available from: https://www.sciencedirect.com/science/article/pii/S0010482521001839.
[69] S.G. Patel, E.J. Sayers, L. He, R. Narayan, T.L. Williams, E.M. Mills, et al., Cell-penetrating peptide sequence and modification dependent uptake and subcellular distribution of green florescent protein in different cell lines [Internet], Sci. Rep. 9 (1) (2019) 6298, https://doi.org/10.1038/s41598-019-42456-8.
[70] I. Botos, D.M. Segal, D.R. Davies, The structural biology of Toll-like receptors [Internet], Structure 19 (4) (2011) 447–459, https://doi.org/10.1016/j.str.2011.02.004.
[71] L. Cao, J. Lou, S.Y. Chan, H. Zheng, C. Liu, S. Zhao, et al., Rapid evaluation of COVID-19 vaccine effectiveness against symptomatic infection with SARS-CoV-2 variants by analysis of genetic distance [Internet], Nat. Med. 28 (8) (2022) 1715–1722, https://doi.org/10.1038/s41591-022-01877-1.
[72] S.I. Richardson, P. Kgagudi, N.P. Manamela, H. Kaldine, E.M. Venter, T. Pillay, et al., Fc effector activity and neutralization against SARS-CoV-2 BA.4 is compromised in convalescent sera, regardless of the infecting variant [Internet], bioRxiv (2022). Available from: https://www.biorxiv.org/content/early/2022/07/15/2022.07.14.500042.